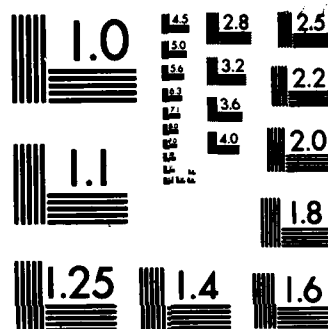MICROCOPY RESOLUTION TEST CHART
NATIONAL BUREAU OF STANDARDS-1963-A

DNA 6195T

# SINGLE EVENT UPSET PHENOMENA FROM HIGH ENERGY NEUTRONS

Mission Research Corporation
1720 Randolph Road, SE
Albuquerque, New Mexico 87106

1 December 1981

Topical Report for Period 1 January 1981—1 December 1981

CONTRACT No. DNA 001-80-C-0140

APPROVED FOR PUBLIC RELEASE;
DISTRIBUTION UNLIMITED.

Prepared for
Director
DEFENSE NUCLEAR AGENCY
Washington, DC 20305

DTIC
ELECTE
AUG 1 1 1983
S
B

83 07 28 034

| REPORT DOCUMENTATION PAGE | | READ INSTRUCTIONS BEFORE COMPLETING FORM |
|---|---|---|
| 1. REPORT NUMBER<br>DNA 6195T | 2. GOVT ACCESSION NO.<br>AD-A131 217 | 3. RECIPIENT'S CATALOG NUMBER |
| 4. TITLE (and Subtitle)<br><br>SINGLE EVENT UPSET PHENOMENA FROM HIGH ENERGY NEUTRONS | | 5. TYPE OF REPORT & PERIOD COVERED<br>Topical Report for Period<br>1 Jan 81—1 Dec 81 |
| | | 6. PERFORMING ORG. REPORT NUMBER<br>AMRC-R-312 |
| 7. AUTHOR(s)<br><br>R. L. Pease and J. P. Raymond | | 8. CONTRACT OR GRANT NUMBER(s)<br><br>DNA 001-80-C-0140 |
| 9. PERFORMING ORGANIZATION NAME AND ADDRESS<br>Mission Research Corporation<br>1720 Randolph Road, S. E.<br>Albuquerque, New Mexico 87106 | | 10. PROGRAM ELEMENT PROJECT TASK AREA & WORK UNIT NUMBERS<br><br>Subtask X99QAXVB201-02 |
| 11. CONTROLLING OFFICE NAME AND ADDRESS<br>Director<br>Defense Nuclear Agency<br>Washington, DC 20305 | | 12. REPORT DATE<br>1 December 1981 |
| | | 13. NUMBER OF PAGES<br>64 |
| 14. MONITORING AGENCY NAME & ADDRESS(if different from Controlling Office) | | 15. SECURITY CLASS (of this report)<br><br>UNCLASSIFIED |
| | | 15a. DECLASSIFICATION DOWNGRADING SCHEDULE<br>N/A since UNCLASSIFIED |

16. DISTRIBUTION STATEMENT (of this Report)

Approved for public release; distribution unlimited.

17. DISTRIBUTION STATEMENT (of the abstract entered in Block 20, if different from Report)

19. KEY WORDS (Continue on reverse side if necessary and identify by block number)

Single Event Upset
Neutron Effects
Nuclear Radiation Environments
Radiation Transport                      SEU

20. ABSTRACT (Continue on reverse side if necessary and identify by block number)

The susceptibility of circumvented and uncircumvented endoatmospheric and exoatmospheric systems to neutron induced (single event upsets) has was con- sidered in very general terms of nuclear weapon threat and system configura- tion.

For both exoatmospheric and endoatmospheric uncircumvented systems it appears that transient upset effects will be dominated by effects (continued)

DD FORM 1473  EDITION OF 1 NOV 65 IS OBSOLETE

20. Abstract (continued)

_cont →_

of the prompt ionization pulse. In the worst case neutron-induced SEUs are comparable to the upset levels of the prompt ionization pulse. For current microelectronic components the neutron-induced SEUs do not need to be explicitly considered for uncircumvented systems. The relative suscepti- bilities should be reviewed with the evolution of microcircuit technology, particularly for possible preferential sensitivity to the localized ionization of a neutron-induced reaction compared to bulk ionization sensitivity.

For circumvented systems there is clearly a potential consideration for exoatmospheric systems and a possible consideration for endoatmospheric sys- tems. Given the threat, microcircuit susceptibility and system performance parameters the calculation of potential concern for a circumvented exoatmos- pheric system is relatively straightforward. If a window of susceptibility exists, two immediate hardening approaches can be considered: 1) increase the system defined electronics recovery time, and/or 2) increase the sensitivity of the system radiation circumvention detectors. The accepta- bility of either of those hardening approaches depends critically on many system performance and threat parameters. The trade-off issues may not necessarily be easily susceptible to resolution.

The high atmospheric concern is comparable to the exoatmospheric case. In some cases the relative neutron transport can be slightly enhanced over the prompt gamma pulse transport. The total prompt ionization pulse is also reduced by the increased attenuation of the low energy photons. The relative decrease in the prompt ionization pulse is, however, relatively unimportant for a circumvented system.

## TABLE OF CONTENTS

# LIST OF ILLUSTRATIONS

## LIST OF TABLES

# SECTION 1

# INTRODUCTION

1-1      BACKGROUND.

High energy neutrons can cause upsets in modern complex microcir-
cuits at exposure levels much less than necessary for significant permanent
damage. Electronic systems using microcircuits are hardened to the tran-
sient effects associated with the pulsed ionization and permanent damage
effects of the total ionization and neutron fluence of the nuclear weapon
radiation environment. The question is whether current hardening tech-
niques are sufficient to protect a system from deleterious single event
upsets.

Recent experiments[1-5] in Single Event Upset (SEU) phenomena have ver-
ified the susceptibility of nMOS dynamic RAMs and nMOS microprocessors for
high energy (nominally 14 MeV) neutrons. The mechanism is ionization in a
critical volume of a memory cell deposited by an alpha particle from an
inelastic collision between an incident neutron and a silicon atom. The
$(n,\alpha)$ cross section is ~100 mb for neutron energies above 5-6 MeV. A 14
MeV neutron can produce alphas with energies between 7.8 and 11 MeV. Only
2.27 MeV of deposited ionization energy in silicon is required per 0.1 pC
of charge. The critical charge for SEUs in many VLSI devices, both
memories and random logic, is in the range of 0.1 to 1 pC[6,7].

Since it has become well established that 14 MeV neutrons can cause
SEUs in large memories and microprocessors, the impact of this phenomena
must be established for weapon systems that have to be hardened to radia-
tion from thermonuclear sources.

The event rate for 14 MeV neutrons ranges from one upset per $10^6$ neu-
trons/cm$^2$ to one upset per $5\times10^8$ n/cm$^2$ for nMOS dynamic memories[2]
and between one upset per $8\times10^{10}$ to one per $2\times10^{12}$ n/cm$^2$ for nMOS
microprocessors[3]. Therefore, SEUs from 14 MeV neutrons can occur at

5

neutron fluence levels well below the levels required to produce significant long term displacement damage.

1-2      SCOPE.

Three basic approaches are used in hardened system design:

1) Operation through a Nuclear Weapons Environment (NWE) exposure without interruption in system performance.

2) Operation interrupted but restored automatically or manually following the NWE exposure.

and

3) Functional operation maintained through the NWE exposure with automatic correction for radiation-induced transient effects (i.e., circumvention).

In the first case, conventional hardening insures that no critical transient effects will occur for any pulsed ionizing radiation exposure up to a critical radiation intensity. Systems in this class would include those hardened for operation through a relatively low-level NWE exposure, or a circumvented system for exposures up to the system-defined circumvention exposure level. The critical SEU question is whether it is possible to get a sufficiently high neutron exposure for the pulsed ionizing radiation exposure allowed within the hardened design.

The second case (i.e., automatic or manual restoration of system operation) has not been considered explicitly in this study. Neutron-induced SEUs from the weapon environment may increase the number of system interruptions. The significance of the increase will, however, depend critically on detailed system threat scenarios and performance requirements

not considered in this study.  Systems of specific concern could include
manned aircraft systems operating at high altitude.

The third case addresses the circumvented system for which
radiation-induced errors from the NWE prompt ionization pulse are acknow-
ledged and corrected.  The critical SEU question is the possibility of
neutron-induced SEUs occurring after the system assumes normal electrical
operation of the semiconductor components.  The concern is that a neutron
pulse of sufficient fluence to cause SEUs will arrive at a time when the
system assumes normal electrical operation.  It is also necessary that the
overall ionization concomitant with the neutron pulse is insufficient to
re-initiate system circumvention.

From a system perspective we have considered systems operated
within or beyond the atmosphere.  If both the system and weapon are endo-
atmospheric, the scattering of neutrons and gamma rays are important as
well as the production of ionization from the neutron transport.  For exo-
atmospheric systems and threats we only have to consider the unscattered
dispersion of the NWE prompt ionization and neutron pulses.

1-3      SUMMARY OF RESULTS.

The susceptibility of circumvented and uncircumvented endoatmos-
pheric and exoatmospheric systems to neutron induced single event upsets
has been considered in very general terms of nuclear weapon threat and sys-
tem configuration.

For both exoatmospheric and endoatmospheric uncircumvented sys-
tems it appears that transient upset effects will be dominated by effects
of the prompt ionization pulse.  In the worst case neutron-induced SEUs are
comparable to the upset levels of the prompt ionization pulse.  For current
microelectronic components the neutron-induced SEUs do not need to be
explicitly considered for uncircumvented systems.  The relative

susceptibilities should be reviewed with the evolution of microcircuit technology, particularly for possible preferential sensitivity to the localized ionization of a neutron-induced reaction compared to bulk ionization sensitivity.

For circumvented systems there is clearly a potential consideration for exoatmospheric systems and a possible consideration for endoatmospheric systems. Given the threat, microcircuit susceptibility and system performance parameters the calculation of potential concern for a circumvented exoatmospheric system is relatively straightforward. If a window of susceptibility exists, two immediate hardening approaches can be considered: 1) increase the system defined electronics recovery time, and/or 2) increase the sensitivity of the system radiation circumvention detectors. The acceptability of either of those hardening approaches depends critically on many system performance and threat parameters. The trade-off issues may not necessarily be easily susceptible to resolution.

The high atmospheric concern is comparable to the exoatmospheric case. In some cases the relative neutron transport can be slightly enhanced over the prompt gamma pulse transport. The total prompt ionization pulse is also reduced by the increased attenuation of the low energy photons. The relative decrease in the prompt ionization pulse is, however, relatively unimportant for a circumvented system.

## SECTION 2

## UNCIRCUMVENTED SYSTEM - EXOATMOSPHERIC

When both the system and weapon are exoatmospheric (for example, a satellite exposure to a high altitude burst) the photon and neutron transport are without attenuation. The prompt gamma ionization dose from a "typical" thermonuclear weapon is given by,

$$\gamma_{(prompt)} \simeq \frac{9 \times 10^4}{R^2} \text{ rads(Si)/kiloton} \tag{1}$$

where R is the slant range between the weapon and the system in kilo-meters. The prompt dose delivered to the microcircuits may also include an additional component due to X-rays which depends on the specific weapon and attenuation of the external X-ray environment by the system structure. In this analysis we will consider only the prompt gamma component which will be the lower limit of the prompt ionizing dose. Using the lower limit to the prompt ionizing dose will give an upper limit to the expected high energy neutron fluence for a given prompt ionization upset level of the microcircuit.

The total neutron fluence for a "typical" thermonuclear weapon is given approximately as,

$$\phi_n \simeq \frac{1.6 \times 10^{12}}{R^2} \text{ n/cm}^2 - \text{kiloton (E>0)} \tag{2}$$

where R is the slant range in kilometers. In this analysis, however, we are interested only in neutrons of sufficient energy to cause a single event upset by a direct n-$\alpha$ reaction with a silicon atom. Assuming a neu-tron energy threshold of 4 MeV for the silicon n-$\alpha$ reaction, and a "typi-cal" neutron energy spectrum for a thermonuclear weapon as shown in Table I,[8] the neutron fluence for energies greater than 4 MeV is approximately 0.167 of the total fluence so,

**Table 1.** Normalized neutron energy outputs for different energy groups for a thermonuclear burst.[8]

| GROUP | NEUTRON ENERGIES (MEV) | FRACTION IN GROUP FOR THERMONUCLEAR WEAPON |
|---|---|---|
| 1 | 1.6905+01 - 1.9640+01 | 0.0 |
| 2 | 1.4918+01 - 1.6905+01 | 0.0 |
| 3 | 1.4191+01 - 1.4918+01 | 1.88714-02 |
| 4 | 1.3840+01 - 1.4191+01 | 9.34254-03 |
| 5 | 1.2840+01 - 1.3840+01 | 2.66169-02 |
| 6 | 1.2214+01 - 1.2840+01 | 1.66622-02 |
| 7 | 1.1052+01 - 1.2214+01 | 1.63678-02 |
| 8 | 1.0000+01 - 1.1052+01 | 1.23974-02 |
| 9 | 9.0484+00 - 1.0000+01 | 7.48258-03 |
| 10 | 8.1873+00 - 9.0484+00 | 6.82320-03 |
| 11 | 7.4082+00 - 8.1873+00 | 6.77521-03 |
| 12 | 6.3763+00 - 7.4082+00 | 1.03201-02 |
| 13 | 4.9659+00 - 6.3763+00 | 1.80706-02 |
| 14 | 4.7237+00 - 4.9659+00 | 3.61700-03 |
| 15 | 4.0657+00 - 4.7237+00 | 1.24302-02 |
| 16 | 3.0119+00 - 4.0657+00 | 2.60380-02 |
| 17 | 2.3852+00 - 3.0119+00 | 2.37305-02 |
| 18 | 2,3069+00 - 2.5852+0C | 3.74662-03 |
| 19 | 1.8268+00 - 2.3069+00 | 2.56418-02 |
| 20 | 1.1080+00 - 1.8268+00 | 6.44472-02 |
| 21 | 5.5023-01 - 1.1080+00 | 8.84954-02 |
| 22 | 1.5764-01 - 5.5023-01 | 9.13765-02 |
| 23 | 1.1109-01 - 1.5764-01 | 1.16335-02 |
| 24 | 5.2475-02 - 1.1100-01 | 1.10777-01 |
| 25 | 2.4788-02 - 5.2475-02 | 5.40049-02 |
| 26 | 2.1875-02 - 2.4788-02 | 5.68196-03 |
| 27 | 1.0333-02 - 2.1875-02 | 9.26377-02 |
| 28 | 3.3546-03 - 1.0333-02 | 1.16267-01 |
| 29 | 1.2341-03 - 3.3546-03 | 7.38166-02 |
| 30 | 5.8295-04 - 1.2341-03 | 2.32454-02 |
| 31 | 1.0130-04 - 5.8295-04 | 2.02810-02 |
| 32 | 2.9023-05 - 1.0130-04 | 1.90145-03 |
| 33 | 1.0677-05 - 2.9023-05 | 0.0 |
| 34 | 3.0590-06 - 1.0677-05 | 0.0 |
| 35 | 1.1254-06 - 3.0590-06 | 0.0 |
| 36 | 4.1400-07 - 1.1234-06 | 0.0 |
| 37 | 1.0000-11 - 4.1400-07 | 0.0 |
| | | Total: 1.00000 |

10

$$\Phi_{n(>4 \text{ MeV})} \simeq \frac{2.7 \times 10^{11}}{R^2} \text{ n/cm}^2 - \text{kiloton} \qquad (3)$$

The expressions for the prompt ionizing dose and high energy neutron fluence are plotted in Figure 1.

Since both the prompt dose and high energy neutron fluence vary linearly with weapon yield and are both inversely proportional to $R^2$, their ratio is,

$$\frac{\Phi_n(>4 \text{ MeV})}{\gamma_p} \simeq 3 \times 10^6 \frac{\text{n/cm}^2 (E>4 \text{ MeV})}{\text{rad(Si)}} \qquad (4)$$

and the ratio is independent of weapon yield and range. Thus if the total prompt dose was 1 rad(Si) the associated high energy neutron would be $3 \times 10^6$ n/cm$^2$ (E>4 MeV). If a microcircuit had a prompt ionization upset level greater than 1 rad(Si) and experienced neutron-induced single event upset at $3 \times 10^6$ n/cm$^2$ the circuit susceptibility would be determined by the neutron SEUs.

The pulsed ionization-induced upset level in microcircuits is a function of the radiation pulse width. For some microcircuits the circuit time constants are long compared to the typical radiation pulse width and the upset level can be defined as dependent on the total prompt dose. Dose-dependent microcircuit types include dynamic MOS memories/microprocessors, dynamic bipolar memories and CCD arrays for radiation pulse widths of less than ~1 μs. Critical total dose upset levels for dynamic MOS memories are on the order of 0.1-10 rads(Si). The neutron exposure consistent with the range of total dose upset levels in dynamic MOS memories would be on the order of $3 \times 10^5$ to $3 \times 10^7$ n/cm$^2$ (E>4 Mev) where the higher neutron fluence corresponds to the least sensitive array to total dose-induced upset.
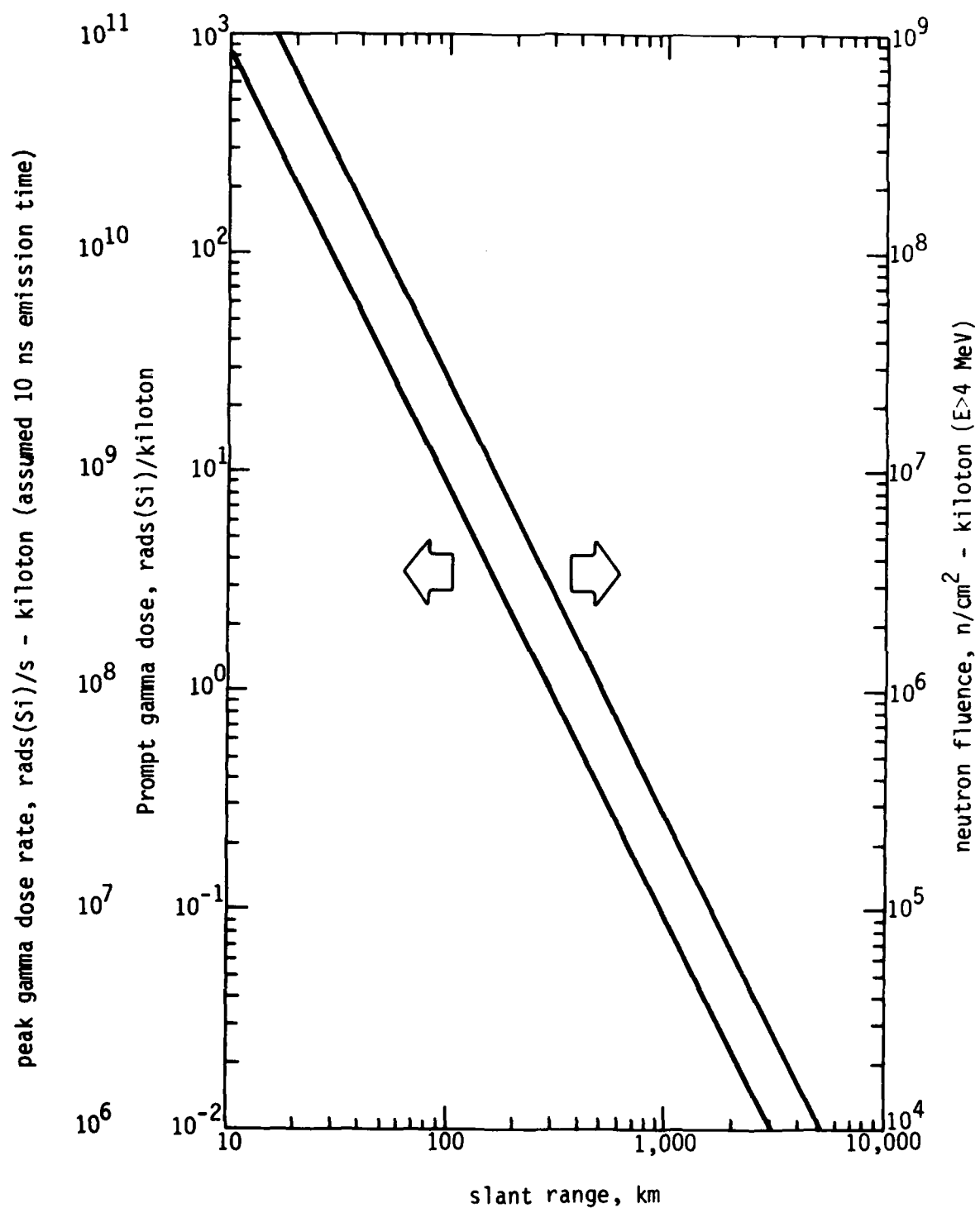
11

Figure 1. Exoatmospheric high energy fluence and prompt ionization dose.

Experimentally, 14 MeV neutron-induced upset levels measured on dynamic n-MOS RAMs vary from $\sim 10^8$ - $5 \times 10^9$ n/cm$^2$ for 4 k memories, $\sim 10^7$ - $5 \times 10^9$ n/cm$^2$ for 16 k memories, and $\sim 6 \times 10^5$ - $10^6$ n/cm$^2$ for early 64 k memories.[1-5] No data are available but it seems reasonable to assume that the pulsed ionization total dose upset on the large memories is also relatively low (perhaps 0.1 - 1 rad(Si)).

In comparing the estimated nuclear weapon high energy neutron fluence and prompt ionization dose to dynamic RAM data, we must estimate the relative effects of the 4-14 MeV weapon spectrum to the 14 MeV experimental data and our lower bound of the prompt ionization exposure. The neutron fluence required for upset increases with decreasing energy to the 4 MeV threshold. As a first-order estimate we assumed that the critical weapon fluence was one-half as effective as the 14 MeV monoenergetic exposure.

The comparison of neutron and prompt ionization upset in dynamic random-access memories is summarized in Table 2. For the 4 k and 16 k d-RAMs it appears clear that the upset is dominated by the prompt ionization pulse. The prompt ionization and neutron SEU levels are close for the 64 k RAM but additional prompt ionization would probably clearly push the dominant upset to that of the prompt ionization pulse. The 64 k d-RAM is a sensitive device to single event upset and it might be expected that the SEU rate from high energy protons and cosmic rays would prohibit application in a satellite system.

The pulsed ionization transient upset levels for static semiconductor memories and microcircuits is on the order of $2 \times 10^7$ to $5 \times 10^8$ rads (Si)/s for pulse widths less than 100 ns and varies roughly with the square root of the pulse width. Assuming weapon pulse width of 20 ns, the critical prompt gamma dose would be on the order of 0.4 to 10 rads (Si) and the associated critical neutron upset fluence would be on the order of $6 \times 10^3$ - $3 \times 10^5$ n/cm$^2$ ($>4$ MeV). There is very little data on the neutron-induced upset. An upset level of $\sim 3 \times 10^8$ n/cm$^2$ ($E \simeq 14$ MeV) was reported

13

| | 14 MeV fluence for SEU $n/cm^2$ | Equiv. NW fluence >4 MeV $n/cm^2$ | Estimated critical $\gamma_{uc}$ rads (Si) | $\Phi_n$ (>4 Mev) Assoc. with $\gamma_{uc}$ $n/cm^2$ |
|---|---|---|---|---|
| 4 k d-RAM | $10^8 - 5 \times 10^9$ | $2 \times 10^8 - 10^{10}$ | 2 | $6 \times 10^6$ |
| 16 k d-RAM | $10^7 - 5 \times 10^9$ | $2 \times 10^7 - 10^{10}$ | 0.5 | $1.5 \times 10^6$ |
| 64 k d-RAM | $6 \times 10^5 - 10^6$ | $1 - 2 \times 10^6$ | 00.1 | $3 \times 10^5$ |
| 4 k s-RAM | $\sim 3 \times 10^8$ | $\sim 6 \times 10^8$ | $\sim 2*$ | $6 \times 10^6$ |

*upset level is pulse width dependent, a 20 ns, $10^8$ rads(Si)/s pulse was assumed.

Table 2. Comparison of RAM measured SEU and NWE neutron fluences.

for the Intel 4 k (2147) static RAM.  The comparison of prompt ionization
and neutron SEU for the static RAM is also included in Table 2.  In this
case it appears that the upset is clearly dominated by the prompt ioniza-
tion pulse.

In summary, it appears that for exoatmospheric systems and NWE
threats that microcircuits will upset from the prompt ionization pulse at
exposure levels lower than those required for neutron-induced upset for
contemporary digital microelectronic semiconductor arrays.  Reported
neutron-induced upset levels for advanced, high density dynamic semiconduc-
tor memories are near upper limit estimated NWE levels but their relative
sensitivity depends on the trend in pulsed ionization upset levels.  From
this analysis it appears that NWE neutron-induced single event upsets do
not add a significant susceptibility to digital microelectronics in exoat-
mospheric systems which are either uncircumvented or circumvented systems
at pulsed ionizing exposure levels below the circumvention level.

# SECTION 3

## CIRCUMVENTED SYSTEM - EXOATMOSPHERIC

The next case of concern is that of an exoatmospheric circum-
vented system such as a satellite or strategic missile in flight. We will
assume that the prompt ionization pulse is of sufficient intensity to ini-
tiate system circumvention. For the purpose of this discussion, circumven-
tion can be described as a system design such that the radiation pulse is
detected and transient upsets of the digital microelectronics are allowed
with the exception of critical data values. After a predetermined time, it
is assumed that transient effects in the electronics have decayed and nor-
mal system operation can be resumed. An additional time interval is
required to update the system and complete recovery. The circumvention
time is normally defined as the interval between initiation and recovery.
The critical time for neutron-induced single event upsets, however, is
after normal electrical performance is assumed as shown in Figure 2.
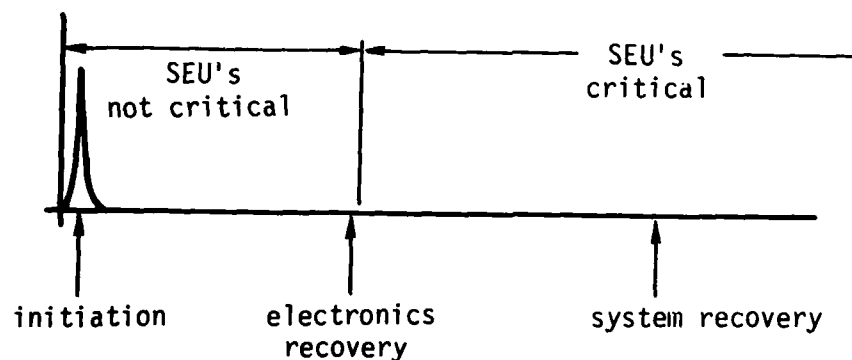


Figure 2. Assumed timing sequence for a circumvented system.

Critical parameters for neutron-induced SEUs in a circumvented
system are:

1) the time of flight of the neutron pulse compared to the elec-
tronics recovery time and,

2) the high energy (>4 MeV) neutron fluence.

16

The neutron time of flight is shown in Figure 3 as a function of range and neutron energy. Because the gamma pulse travels at the speed of light, it is reasonable to assume that the delay between system circumvehtion and the leading edge of the neutron pulse is approximately equal to the 14 MeV neutron time of flight.

Using the $1/R^2$ dispersion for neutrons in the absence of scattering and the high energy neutron yield for a "typical" thermonuclear weapon (equation 3), the neutron fluence is shown in Figure 4 as a function of time of flight (equivalent to range) for weapons of different yield.

The influence of possible system parameters is illustrated in Figure 5. If we assume that the electronics recovery time is 5 ms, then neutron-induced SEUs occurring earlier will be corrected with the rest of the scrambled electronics memory. If we also assume that the microcircuit sensitivity is $3 \times 10^8$ n/cm$^2$ (E>4 MeV), which is on the order of that observed for an n-MOS static RAM, neutron exposures below the critical upset level will not be of concern even if the neutron pulse arrives later than the electronics recovery time. The window of vulnerability for the system to neutron-induced SEUs, for the assumed parameters would be for thermonuclear weapon exposures of yield greater than 100 kT at ranges greater than approximately 200 km. We feel that a window of vulnerability can exist for circumvented exoatmospheric systems. The degree of existence, or absence, of the window of vulnerability depends strongly on the specific system performance characteristics and threat and no general conclusions can be made.
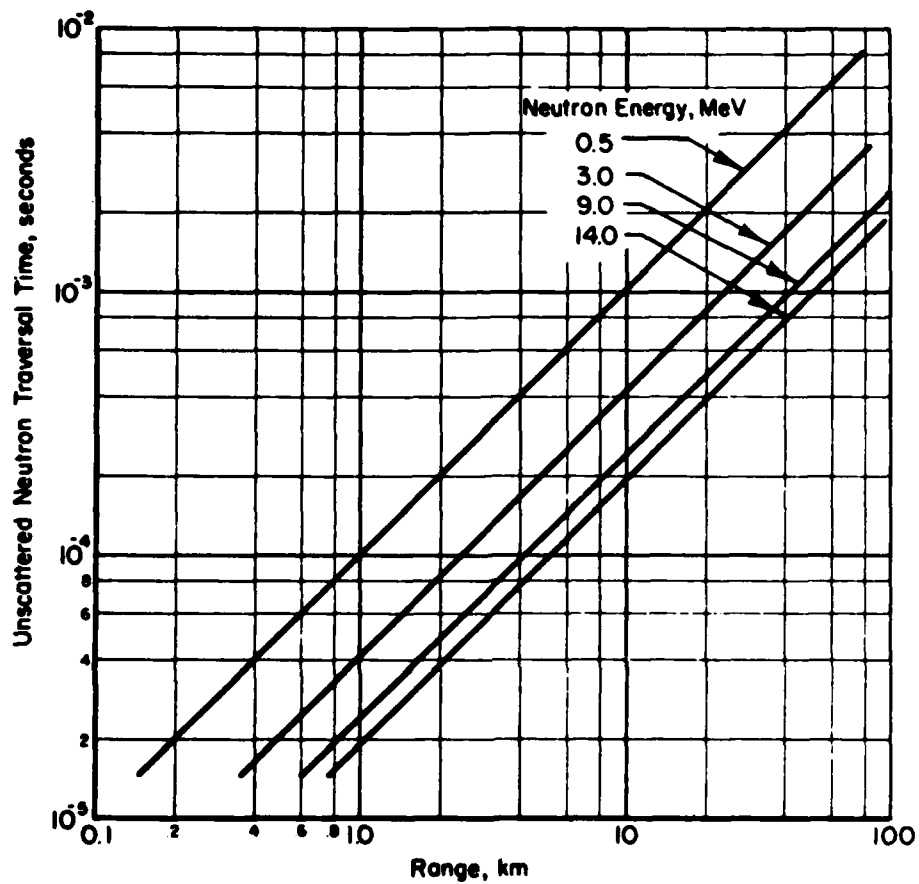
Figure 3. Unscattered neutron traversal time for various monoenergetic source energies as a function of range.
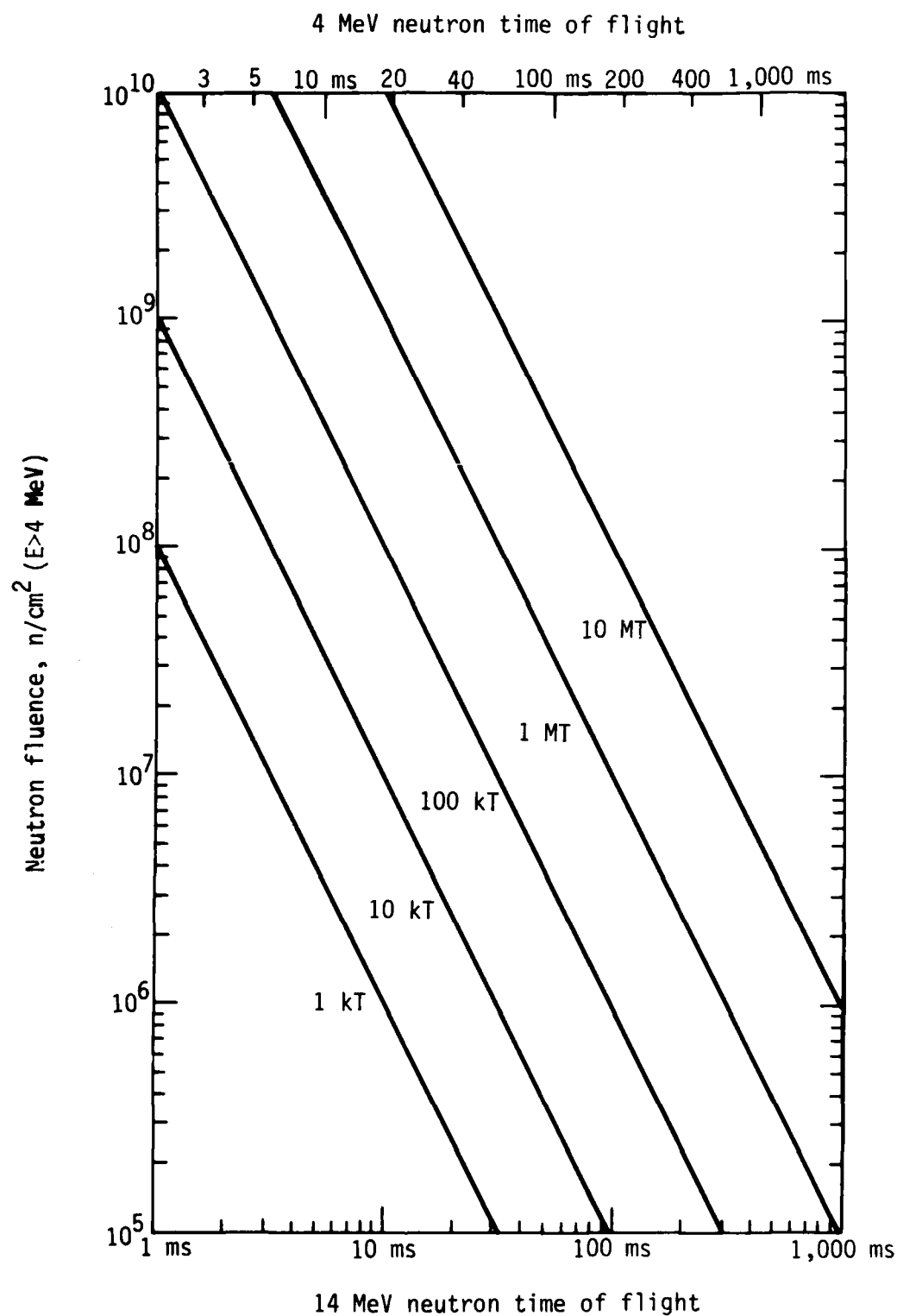
Figure 4. Time-delayed exoatmospheric high energy neutron fluence.
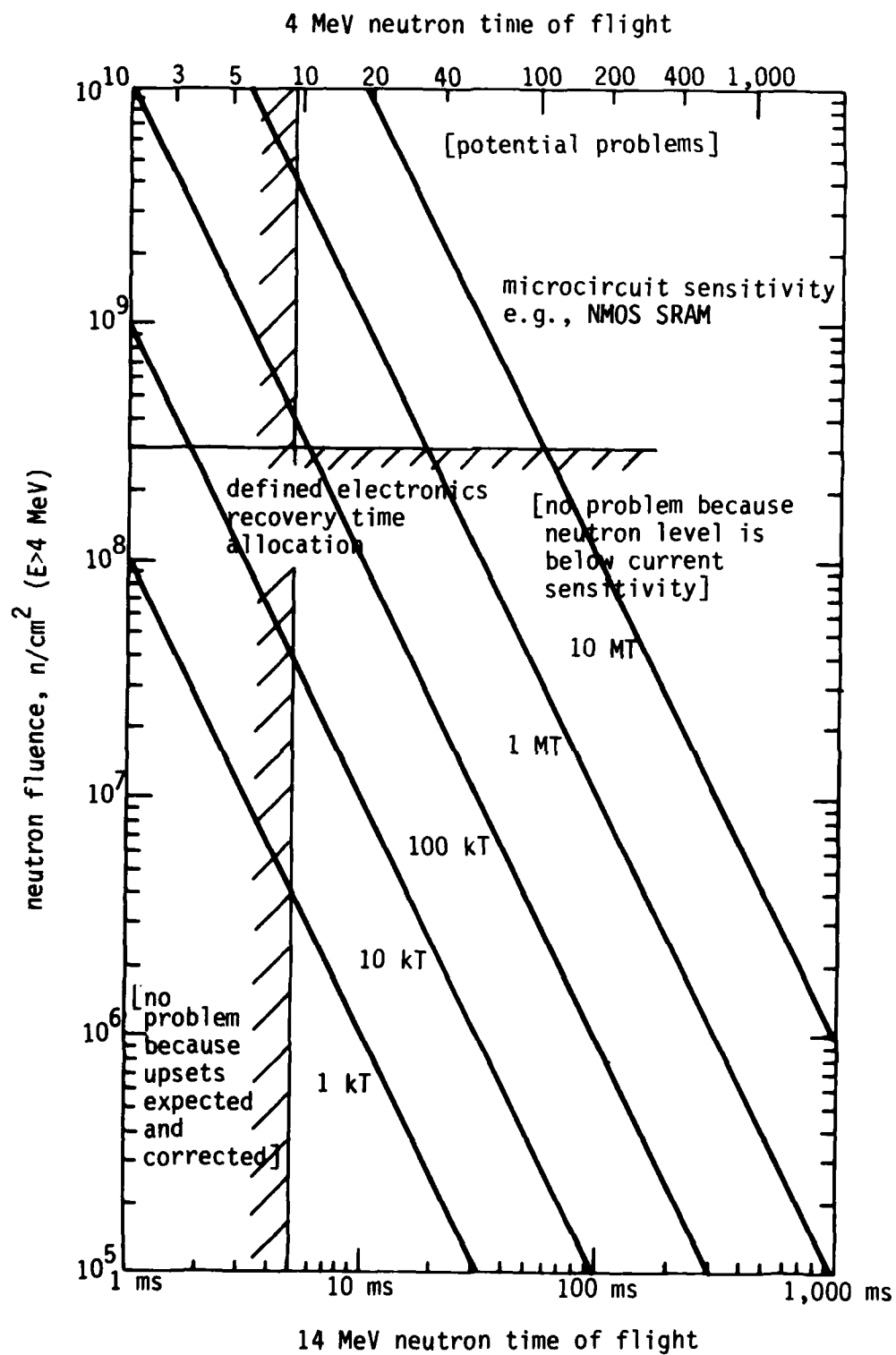
19

Figure 5.   Possible exoatmospheric window of susceptibility.

# SECTION 4

## ENDOATMOSPHERIC SYSTEMS

In the analysis for the exoatmospheric environment, the high energy neutron SEU phenomena was addressed by merely calculating the spherical divergence of the prompt gamma rays and the neutrons. Two cases of interest were established, a) the system does not circumvent and a sufficient number of high energy neutrons arrive at the target to cause SEUs. In this case the arrival time of the neutrons is of no interest. And b) the system circumvents but a sufficient number of high energy neutrons to cause SEUs arrive at the target after it has recovered. In this case the neutron arrival times must be known. If both of these cases are considered for the endoatmospheric environment, then the attenuation of the prompt gamma rays, the attenuation and energy degradation of the neutrons and the time dispersion of the neutrons must be calculated for transport through non-uniform air.

Neutron and gamma ray transport through air has been studied extensively and a large volume of calculated data is available[8-12]. The air transport problem has been addressed with a one dimensional transport code, ANISN, in uniform air and with Monte Carlo calculations in both uniform and non-uniform air. Comparisons between calculations made in uniform and nonuniform air indicate that over a wide range of altitudes and slant ranges, the uniform air calculations can be applied to any endoatmospheric scenario by using the concept of mass integral scaling (MIS). This concept means that the transport of gammas and neutrons is simply a function of how much air mass the radiation must pass through from source to target. In addition to the attenuation through a given air mass, spherical divergence $(1/4\pi R^2)$ must be taken into account in order to determine the prompt gamma dose rate and neutron fluence for a given range and air mass. Thus the radiation environment reaching the target is determined from a relation of the form

$$ENV_T = \frac{S}{4\pi R^2}\, e^{-\mu m_a}$$

where $ENV_T$ is the environment of interest at the target, S is the source strength, R the range, $\mu$ an attenuation coefficient in $cm^2/g$ and $m_a$ the air mass in $g/cm^2$.

If the results of calculations made in uniform air are used to determine the value of $\mu$ and MIS is applied, the results should be within a factor of 2 for most scenarios. Thus, to determine the extent of the high energy neutron SEU phenomena in air, uniform air calculations will be used. The main reason for using the uniform air results is that the available literature for uniform air calculations includes neutron energy and time dependence whereas the nonuniform air results include only the integrated neutron results over the whole energy range. For the SEU phenomena, only the neutrons with energies above ~4 MeV are of interest.

The endoatmospheric scenario can be extrapolated from the exoatmospheric results by including an exponential attenuation factor for a given air mass. Thus for a given scenario in air the range and total air mass must first be determined.

4-1    CALCULATION OF AIR MASS.

The density of air as a function of altitude is assumed to follow an exponential decrease from the sea level value of 1.22 mg/cm^3. Using this relation graphs and nomographs have been established to determine the air mass for a given range and altitude of source and target. For the case where the source is exoatmospheric and directly above the target, the air

22

mass between source and target can be determined for a given target altitude from Figure 6.[13] In this case a simple integration of the variable density from the target altitude to ∞ has been performed. For the case where the source and target are at the same altitude, the air mass can be determined from Figure 7.[13] In this figure the coaltitude is given on the vertical scale and the curves for coaltitude range are given for .5 km to 40 km.

If the source and target are not at the same altitude, then the nomograph given in Figure 8 must be used.[13] Directions for using the nomograph are given in the figure.

Once the range and air mass are determined for a given scenario, then the prompt gamma dose rate and high energy neutron fluence can be determined from the spherical divergence and uniform air transport calculations.

4-2     CALCULATION OF PEAK DOSE RATE IN AIR.

The maximum dose rate, which can result in circumventon, will be due to the prompt gamma rays. Attenuation of the prompt gammas in air, due to the interaction of the gammas with air molecules is given by a total mass attenuation coefficient and a total mass absorption coefficient. Both of these exponential decay factors are energy dependent. The mass attenuation coefficient assumes that all gammas which undergo an interaction in air are removed from the beam. Hence, coherent scattering is not accounted for. The mass absorption coefficient is determined by including coherent scattering and hence the removal cross section is somewhat lower. Table 3 is a list of the mass absorption and mass attenuation coefficients for gammas of various energies in dry air.
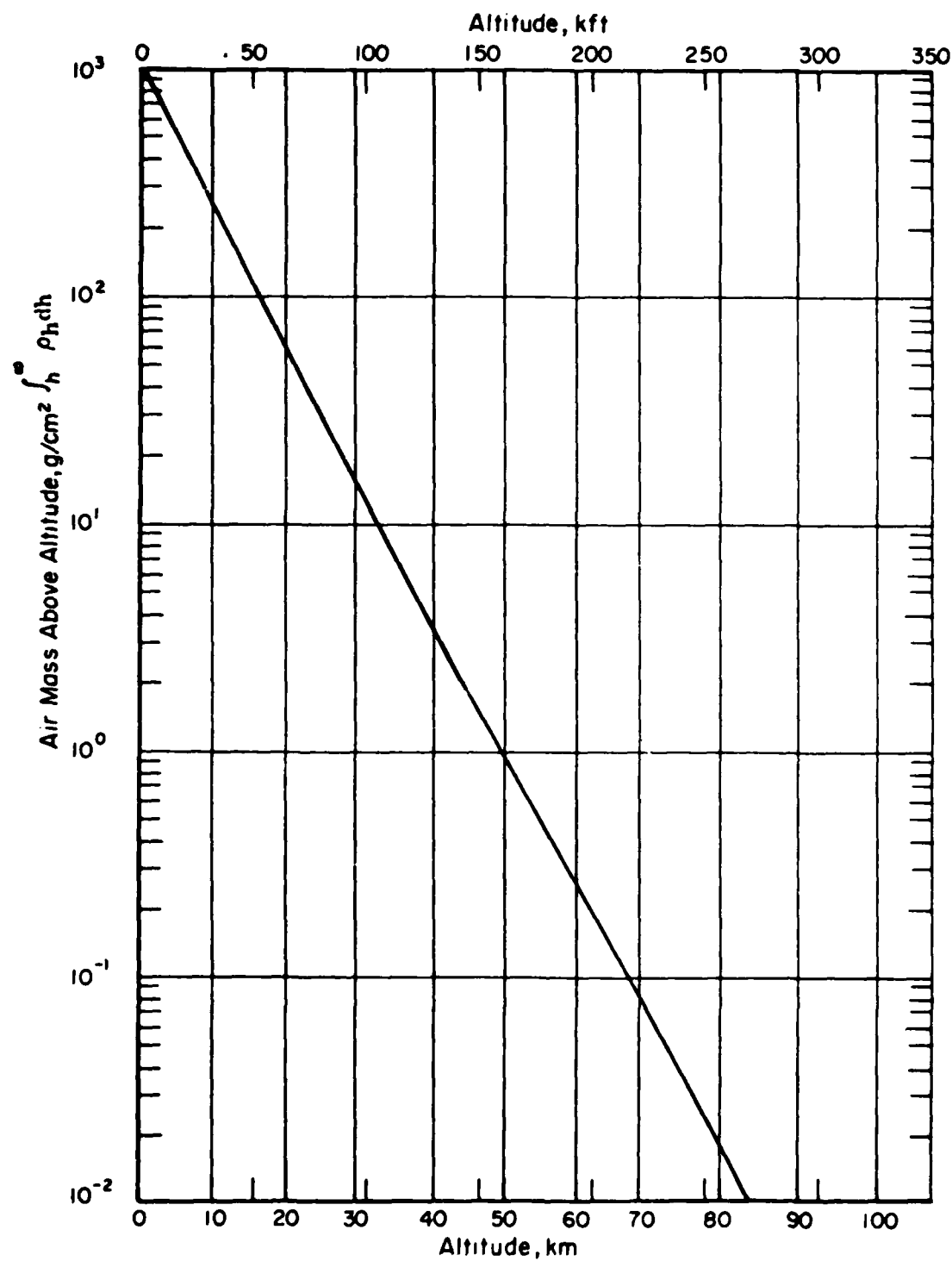
23

Figure 6. The mass of air above each altitude $h \left( \int_h^\infty \rho_h \, dh \right)^{13}$.
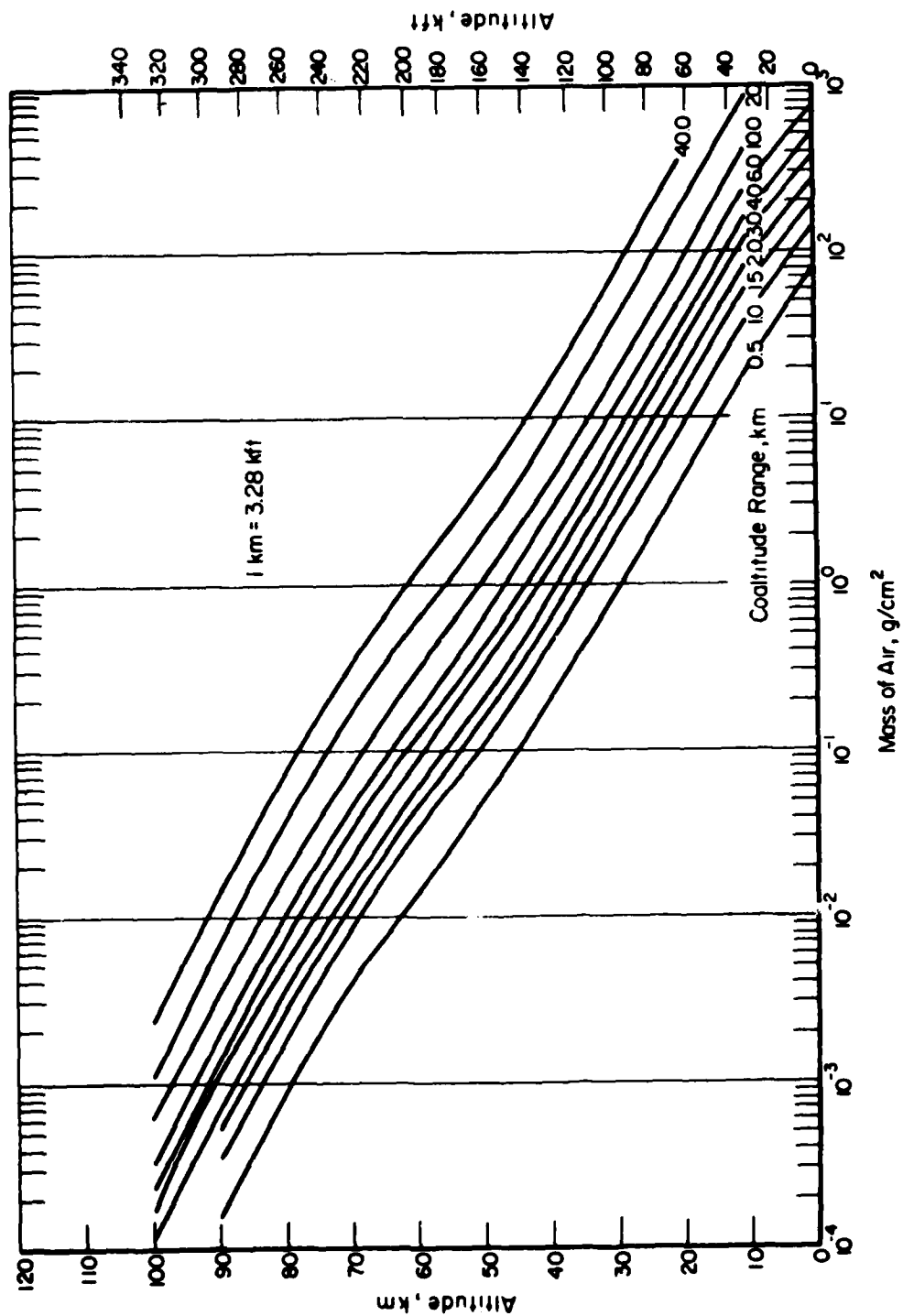
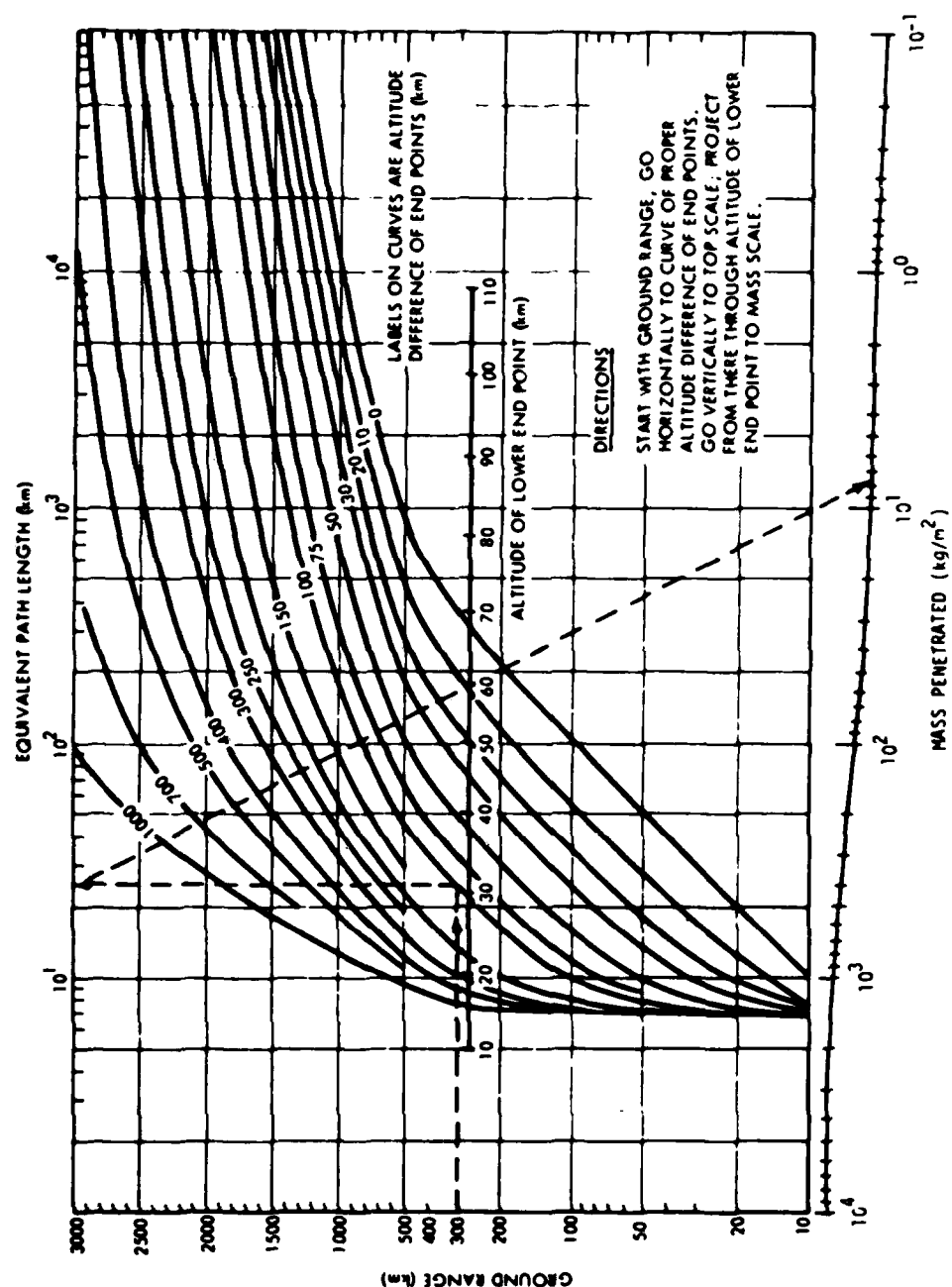Figure 7. Air mass for various coaltitude ranges as a function of altitude.[13]

Figure 8. Computation of mass penetrated between two points in the atmosphere

$1 \text{ kg/m}^2 = .1 \text{ g/cm}^2.$ [13]

Table 3. Total mass-absorption and mass-attenuation cross sections in air for various gamma-ray energies.

| Gamma-Ray Energy (MeV) | Total Mass-Absorption Cross Section (cm²/g) | Total Mass-Attenuation Cross Section (cm²/g) |
|---|---|---|
| 0.5 | 2.95(-2) | 8.65(-2) |
| 1.0 | 2.82(-2) | 6.26(-2) |
| 2.0 | 2.37(-2) | 4.38(-2) |
| 4.0 | 1.92(-2) | 4.06(-2) |
| 6.0 | 1.72(-2) | 2.49(-2) |
| 8.0 | 1.60(-2) | 2.19(-2) |
| 10.0 | 1.54(-2) | 2.01(-2) |

Note: Mass fractions = 0.755 nitrogen, 0.232 oxygen, 0.013 argon.

For the purposes the present calculations, the mass absorption coefficient will be used since it represents a more realistic case. A plot of the attenuation of the prompt gammas as a function of air mass is given in Figure 9 for 0.5, 2 and 10 MeV gammas.

The dose rate from prompt gammas at the target can be determined if the following information is known.

a) Air mass

b) Range

c) Source strength and energy spectrum for weapons type - gammas per kiloton and energy distribution.

d) Emission time of gammas

To convert the gamma flux to dose rate in silicon, the Henderson flux to dose conversion factor is used. For the exoatmospheric calculations the
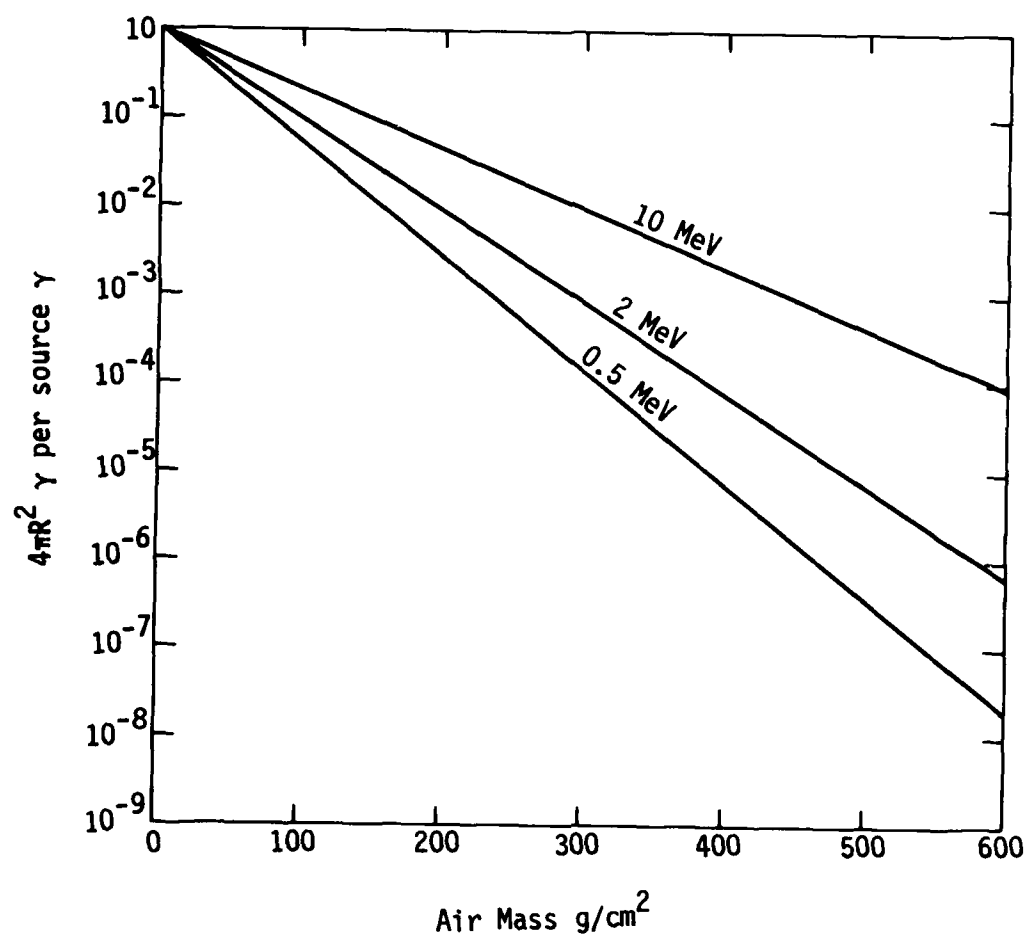
27

Figure 9.   Attenuation of prompt gammas in air.

dose per kiloton versus range was determined from Figure 1. This figure was derived assuming a "typical" thermonuclear source and using the Henderson gamma to dose (Si) conversion for 1 MeV gammas.[13]

## 4-3    HIGH ENERGY NEUTRON TRANSPORT IN AIR.

For the high energy neutron SEU phenomena, the high energy neutron fluence must be determined at the target after transporting through a given air mass. Therefore, not only the total neutron attenuation must be known, but the degradation of the energy spectrum as well. Straker has calculated the angular and energy dependence of neutron transport in uniform dry air from both discrete neutron sources and a typical thermonuclear source.[8] The one-dimensional transport code ANISN was used. Calculations were carried out to 4800 meters (533 g/cm$^2$) for the 12.2-15 MeV source and out to 1800 meters (200 g/cm$^2$) for the thermonuclear source.

Using Straker's results, the $4\pi R^2$ neutrons per source neutron values were calculated for neutron energies greater than 4.06 MeV at the target as a function of air mass. The results are shown in Figure 10 for the 12.2-15 MeV source and the thermonuclear source. The energy spectrum of the thermonuclear source is shown in Table 4.

Also shown in Figure 10 is the attenuation of 1 MeV prompt gammas using the mass absorption coefficient. The results of the neutron transport calculations indicate that for air masses of greater than 100-200 g/cm$^2$ the attenuation of neutrons can be represented fairly well by a constant exponential attenuation factor $\mu_n$ in g/cm$^2$. From the calculated results in Figure 10, neutron attenuation coefficients (removal cross sections) were determined. These are presented in Table 5 for the 12.2-15 MeV and thermonuclear sources.
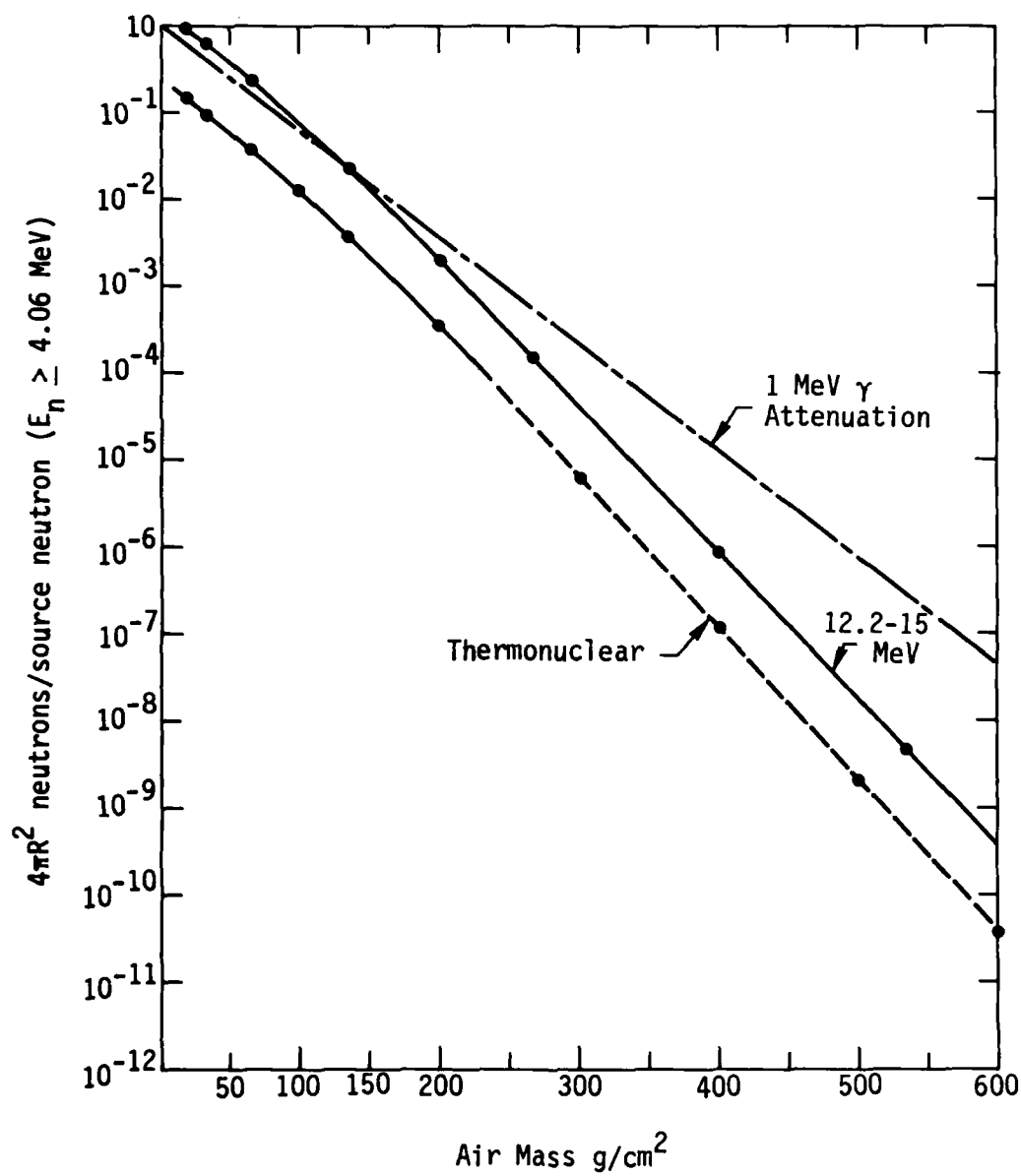
Figure 10. Attenuation of high energy neutrons in air.

Table 4.  Neutron energy spectrum for a thermonuclear source.

| Energy (MeV) | Fraction in Group |
|---|---|
| 12.2-15 | .0706 |
| 10.-12.2 | .0256 |
| 8.19-10. | .0141 |
| 6.36-8.19 | .0147 |
| 4.97-6.36 | .0180 |
| 4.07-4.97 | .0170 |
| 3.01-4.07 | .0260 |
| 2.46-3.01 | .0190 |
| 2.35-2.46 | .0050 |
| 1.83-2.35 | .0280 |
| 1.11-1.83 | .0620 |
| .55-1.11 | .0850 |
| .55 < | .615 |

Table 5.  Neutron attenuation coefficients versus air mass for 12.2-15 MeV and thermonuclear sources.

| 12.2-15 MeV Source | | Thermonuclear Source $(E_n \geq 4.07$ MeV is 16%) | |
|---|---|---|---|
| Air mass $g/cm^2$ | $\mu_n$ $cm^2/g$ | Air mass $g/cm^2$ | $\mu_n$ $cm^2/g$ |
| 33.3 | .0145 | 33.3 | .070 |
| 66.6 | .0221 | 66.6 | .0495 |
| 133 | .0283 | 100 | .0434 |
| 200 | .0311 | 133 | .0418 |
| 266 | .0329 | 200 | .0400 |
| 400 | .0348 | | |
| 533 | .0361 | | |

Although the value of $\mu_n$ is not constant over the entire range of air masses of interest for most scenarios, it is fairly constant above 100 g/cm$^2$. A nominal value of .033 cm$^2$/g could be used for the 12.2-15 MeV source and .040 cm$^2$/g for the thermonuclear source.

## 4-4    TIME DISPERSION OF NEUTRONS.

For the SEU case where the system circumvents, the neutron arrival times must be known. For an exoatmospheric environment, the neutron arrival time is determined from the direct, unscattered neutron time of flight. However for transport in air only a few of the neutrons reach the target without undergoing either an elastic or inelastic collision. Therefore, the arrival becomes dispersed in time. Straker[10] has performed time-dependent Monte-Carlo transport calculations in uniform air for a source 50 ft. above ground. Results are tabulated for the $4\pi R^2$ neutron flux as a function of energy and time for slant ranges up to 1300 meters. Neutron sources were discrete energy bins and a fission spectrum. No calculations were made for a thermonuclear source. In order to determine the time dispersion for the high energy neutrons of interest to SEUs, calculations of the total $4\pi R^2 \emptyset (E_n \geq 4.06$ MeV) have been made versus time for 12.2-15 MeV source. The results are shown in Figure 11 for slant ranges of 700 and 1300 meters. These ranges correspond to 77 and 143 g/cm$^2$ air mass. The two histogram plots in Figure 11 show the fraction of the total high energy neutron fluence reaching the detector for the various time bins. Also shown (shaded area) is the time bin bounded by the direct transit time for the 15 MeV neutrons to the near side of the detector and the transit time for 12.2 MeV neutrons to the far side of the detector. For the 700 meter slant range, the detector extends from 675 to 725 meters and for the 1300 meter slant range, the detector extends from 1225 to 1375 meters. Thus the shaded area represents the maximum range of time of flight for the unperturbed source neutrons. If the nominal time of flight for the time dispersed neutrons is compared to the time of flight for unperturbed neutrons then the arrival times are seen to approximately double for both slant ranges.

ORNL-8289 Vol. II

Monte Carlo Calculations - Source 50 ft. above ground - air density - 1.11 mg/cm$^3$

Source Neutrons 12.2-15 MeV  Neutrons at Detector $E_n \geq 4.06$ MeV.

Slant Range 700 meters, air mass 77 g/cm$^2$,  $4\pi R^2 \phi(E_n \geq 4.06$ MeV$) = .0752$ n/source n

Time in μs
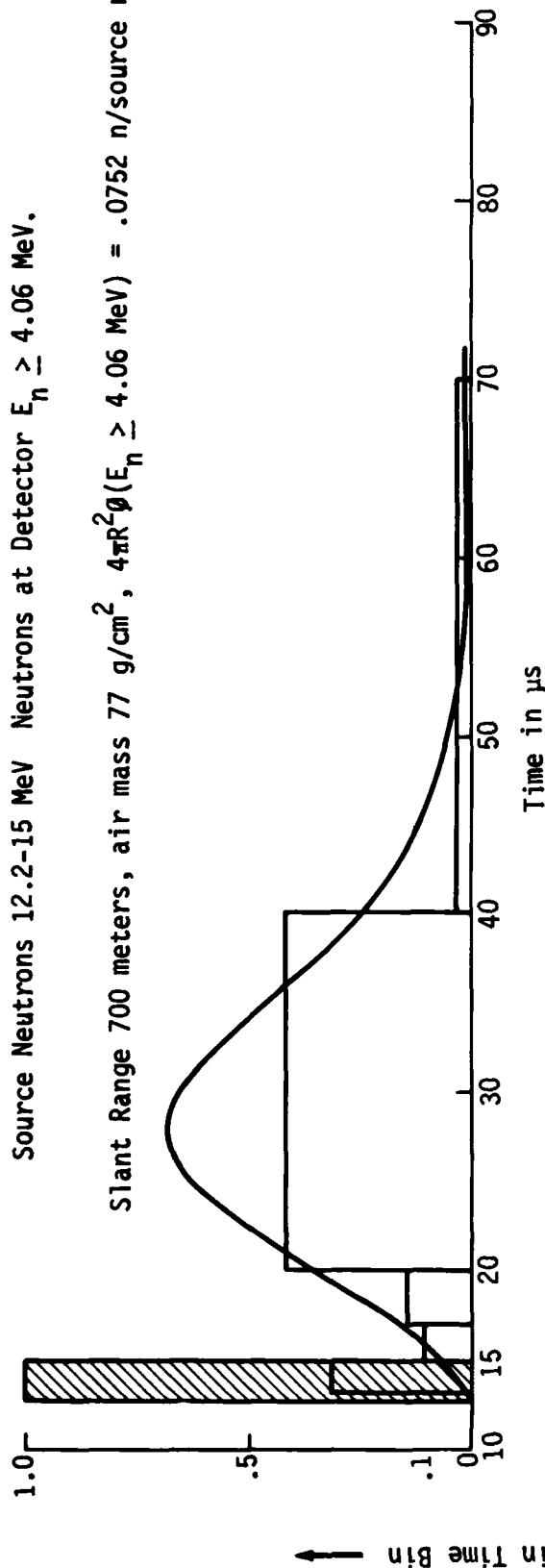
Slant Range 1300 meters, air mass 143 g/cm$^2$,  $4\pi R^2 \phi(E_n \geq 4.06$ MeV$) = .00658$ n/source n

Time in μs

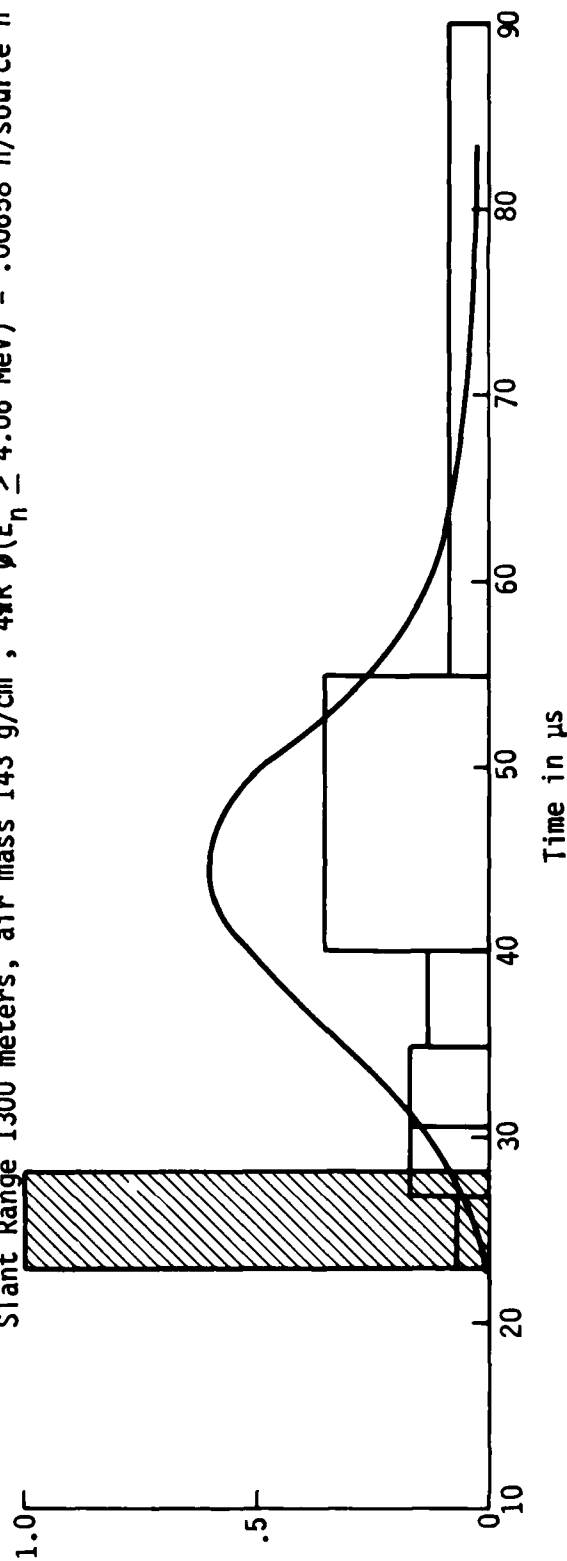Fraction of $\phi(E_n \geq 4.06$ MeV$)$ in Time Bin

Figure 11.  Time dispersion of high energy neutrons.

33

# SECTION 5

## COMPARISON OF EXOATMOSPHERIC AND ENDOATMOSPHERIC ENVIRONMENTS

In the section on the exoatmospheric environment, two sets of curves were developed to determine the high energy neutron fluence from a typical thermonuclear weapon for the two cases, a) no circumvention, and b) circumvention with neutrons arriving after the system has recovered. Using the concept of exponential attenuation in addition to spherical divergence, the exoatmospheric results can be extended to the endoatmospheric environment if the amount of air mass between source and target is known.

For the case where the system does not circumvent, i.e., the peak dose rate from prompt gammas is less than the threshold level for circumvention, the fluence of high energy neutrons reaching the target is reduced from the exoatmospheric calculation by the ratio between high energy neutron attenuation and the prompt gamma ray attenuation.

For example, if the air mass is 300 $g/cm^2$, corresponding to the target at 26,000 ft. and the source is exoatmospheric and directly above the target, then the ratio between the thermonuclear high energy neutron attenuation, $\exp(-\mu_n m_a)$, and the 1 MeV prompt gamma attenuation, $\exp(-\mu_\gamma m_a)$, is .029. Thus the fluence of high energy neutrons in 300 $g/cm^2$ of air would be only .029 times the exoatmospheric fluence for the same circumvent threshold level.

Closer inspection of Figure 10 and the data in Table 5 indicate that this simplified procedure cannot be applied to air masses of less than about 150 $g/cm^2$. For air masses less than this value the high energy neutron attenuation coefficient is not constant. In fact the results for the 12.2-15 MeV source attenuation curve lies slightly above the 1 MeV gamma attenuation curve below 100 $g/cm^2$ air. The thermonuclear curve is displaced downward since only 16% of the source neutrons have energies > 4 MeV to begin with.

34

Based on these results, the following conclusions can be drawn for the endoatmospheric environment for the case where the system does not circumvent:

1) For air masses up to ~150 g/cm$^2$ the high energy neutron fluence will be essentially the same as for the exoatmospheric environment. Thus, Figure 1 can be used for the typical thermonuclear source.

2) For air masses greater than 150 g/cm$^2$, the high energy neutron fluence will be lower than for the exoatmospheric environment. The reduction factor can be estimated from the ratio

$$\frac{e^{-\mu_n m_a}}{e^{-\mu_\gamma m_a}}$$

The second case to consider is the one for which the source is far enough away such that the high energy neutrons arrive after the system has recovered from a circumvention. For this case the time dispersion of the neutrons in the atmosphere as well as the attenuation must be determined. The arrival time for unperturbed neutrons versus range is given in Figure 3 for various monoenergetic neutrons.

For a system off time of only 1 ms the range for 4 MeV to 14 MeV unscattered neutrons is 28 to 52 km. The results of the time dispersion calculations given in Figure 9 indicate that only 30-40% of the high energy neutrons arrive at times greater than twice the unscattered arrival times for ranges up to 1.3 km. Unfortunately, no tablulated data in the open literature could be found for calculations of time dispersion at greater

35

ranges. However it can be assumed that the time dispersion is more a function of air mass than range. The results of Figure 11 extend to 143 $g/cm^2$ air mass. Even if a factor of two increase in dispersion is assumed with only a factor of 3 decrease in high energy neutron fluence then the range can only be reduced to 14-26 km for the high energy neutrons for a 1 ms arrival time. For a 14-26 km range the minimum air mass for an endoatmospheric scenario would be with the source exoatmospheric and the target at some altitude directly below the source. If we assume an altitude of 50,000 ft. for the target, the air mass would be about 120 $g/cm^2$ from Figure 6. Using the attenuation calculations of Figure 10 for the 12.2-15 MeV neutron component, the attenuation of 120 $g/cm^2$ is .038 or a factor of 26 lower than the corresponding exoatmospheric calculation. For a coaltitude scenario at 50,000 ft. the air mass for the coaltitude range of 14-26 km is 230-450 $g/cm^2$. This would correspond to a $6 \times 10^{-4}$ to $10^{-7}$ reduction in high energy neutrons from the exoatmospheric calculation.

Based on the endoatmospheric calculations for the case where the system does circumvent the following conclusions can be drawn.

1) The high energy neutron fluence will be less than the high energy neutron fluence for the exoatmospheric environment.

2) The time dispersion in the atmosphere will not be great enough to significantly reduce the required range between source and target.

3) The minimum amount of air mass for the required range will occur for the scenario where the source is exoatmospheric and directly above the high altitude target.

4) If both source and target are located in the atmosphere, then the air mass for the required range will significantly reduce the high energy neutron fluence.

# SECTION 6

## CONCLUSIONS

Concern for neutron-induced single event upsets compromising the performance of hardened military systems can be listed in order of decreasing concern as follows:

1) Circumvented, exoatmospheric systems.

2) Circumvented, high endoatmospheric systems.

3) Uncircumvented, high endoatmospheric systems.

4) Uncircumvented, exoatmospheric systems.

5) Low endoatmospheric systems.

The degree of concern will be a function of detailed system performance requirements, detailed threat scenarios, and microcircuit SEU susceptibility. Subjectively, the concern for circumvented, exoatmospheric systems seems clear for systems using modern MOS or bipolar semiconductor memories (e.g., $\geq$ 1 k bit/chip). The concern for circumvented, high endoatmospheric systems is not as clear but approaches that of exoatmospheric systems. The concern for uncircumvented and low endoatmospheric systems is not clear and probably represents no significant problem with today's semiconductor components.

Parameters of circumvented system can be adjusted to minimize or eliminate a neutron SEU problem with trade-offs in overall system performance. For example, the defined system recovery time can be increased and/or the radiation detector/circumvention level can be decreased (i.e., increased in sensitivity). If the recovery time is increased, the total circumvention time will increase and the increased "off" time may degrade overall system performance. If the circumvention level is decreased, the number of circumventions for complex threat scenarios may increase, also increasing the system "off" time with possible degradation in system performance.

An alternative approach to system hardening is to employ micro-circuits of acceptable SEU susceptibility. Unfortunately, the trend seems to be an increase in SEU susceptibility as we go toward more complex advanced semiconductor devices. For the specific concern of weapon-environment effects we can at least be confident that the microcircuit susceptibility cannot increase above the limit defined by errors induced by cosmic rays and high energy protons. The cosmic ray and high energy proton SEU susceptibility is a basic operational concern for satellite systems and cosmic ray susceptibility is a potential concern for high altitude avionics.

On balance, neutron-induced single event upsets represent an additional hardening concern for some classes of military systems but do not represent a major concern for the broad range of military systems and does not represent a significant exploitable vulnerability to existing systems.

# REFERENCES

1. Guenzer, C. S., et. al., "Single Event Upsets in RAMs Induced by Protons at 4.2 GeV and Protons and Neutrons below 100 MeV," IEEE Trans. Nuc. Sci., NS-27, No. 6, p. 1485, December 1980.

2. Guenzer, C. S., E. A. Wolicki and R. G. Allas, "Single Event Upset of Dynamic RAMs by Neutrons and Protons," IEEE Trans. Nuc. Sci. NS-26, No. 6, p. 5048, December 1979.

3. Guenzer, C. S., A. B. Campbell and P. Shapiro, "Single Event Upsets in nMOS Microprocessors," IEEE Trans. Nuc. Sci., NS-28, No. 6, December 1981.

4. Bradford, J. N., "Single Event Error Generation by 14 MeV Neutron Reactions in Silicon," IEEE Trans. Nuc. Sci. NS-27, No. 6, p. 1480, December 1980.

5. Petersen, E., "Nuclear reactions in Semiconductors," IEEE Trans. Nuc. Sci., NS-27, No. 6, p. 1494, December 1980.

6. Price, W. E., et. al., "Cosmic Ray Induced Errors in $I^2L$ Microprocessors and Logic Devices," IEEE Trans. Nuc. Sci., NS-28, No. 6, December 1981.

7. May, T. C. and M. H. Woods, "Alpha-Particle-Induced Soft Errors in Dynamic Memories," IEEE Trans. Elec. Dev., ED-26, No. 1, June 1979.

8. Straker, E. A. and M. L. Gritzner, Neutron and Secondary Gamma-Ray Transport in Infinite Hogmogeneous Air, ORNL-4464, Oak Ridge National Laboratory, December 1969.

9. Straker, E. A. and F. R. Mynatt, Calculations of the Effect of the Air-Ground Interface on the transport of Fission Neutrons through the Atmosphere, ORNL-TM-1819, Oak Ridge National Laboratory, 01 November 1967.

10. Straker, E. A., Time-Dependent Neutron and Secondary Gamma-Ray Transport in an Air-Over-Ground Geometry, (2 volumes), ORNL-4289, Oak Ridge National Laboratory, 1968.

11. Shulstad, K. A., An Evaluation of Mass Integral Scaling as Applied to the Atmospheric Radiation Transport Problem, AFWL-TR-76-221, Air Force Weapons Laboratory, Kirtland AFB, New Mexico, December 1976.

REFERENCES (Cont'd)

12. Eamon, J. C., High Altitude Atmospheric Radiation Transport Calcula-
    tions," AFWL-TR-76-142, Air Force Weapons Laboratory, Kirtland AFB,
    New Mexico, August 1976.

# APPENDIX
## LUMPED MODEL ANALYSIS OF TWO-DIMENSIONAL CARRIER COLLECTION

It is generally assumed that the transient current of a reverse-biased p-n junction from a single particle ionization track is a narrow pulse. If the pulse width is short compared to the smallest circuit time constant then the circuit response will be determined by the total collected charge and the details of the waveform are not important. On the other hand, if the pulse width is comparable to the circuit time constants details of the waveform will be important in establishing the circuit upset level.

Charge generated by the particle ionization track in, and near, the junction depletion layer will be collected quickly. Detailed one-dimensional calculations for realistic doping profiles and including effects of hole and electron transport (i.e., funneling) predict a subnanosecond current pulse (Ref. 1-3). This fast current pulse is dominated by carrier collection in the depletion layer which is enhanced by funneling.

Carriers generated deeper in the bulk semiconductor will diffuse to the junction with some time delay before collection. If the bulk semiconductor were ionized uniformly this would be the familiar diffusion component of photocurrent. The diffusion photocurrent decays with a time constant on the order of the minority carrier lifetime. For modern non-gold-doped microcircuits the high resistivity substrate lifetime can be on the order of microseconds. Time constants on this order would be significant in the response of virtually all types of microcircuits.

Intuitively, the diffusion current resulting from a single particle ionization will be less than that observed by uniform carrier generation because of carrier diffusion away from the ionization track (Figure 1). This would suggest a photocurrent pulse which is smaller and narrower than the uniform-ionization photocurrent (Figure 2).

41
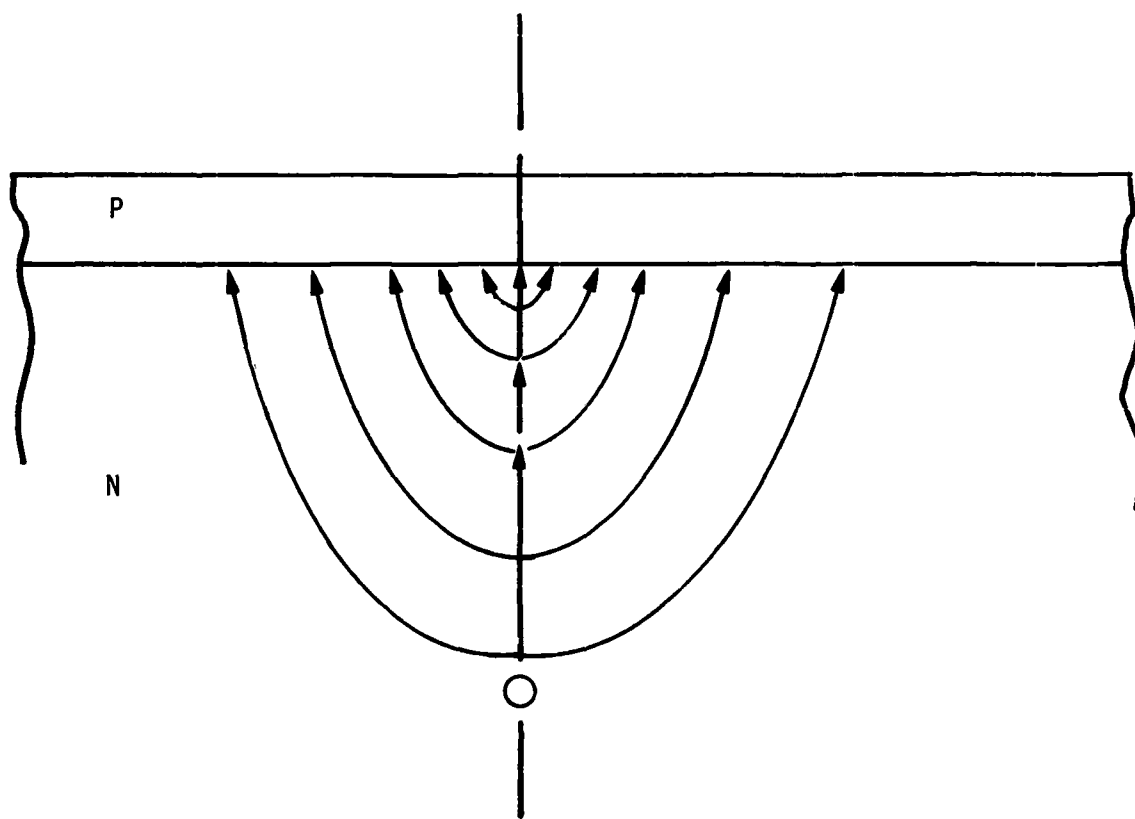
Figure 1. Lateral diffusion of single particle-generated carriers.

assumed single-event photocurrent

diffusion component of single-event
photocurrent (worst-case single-event?)

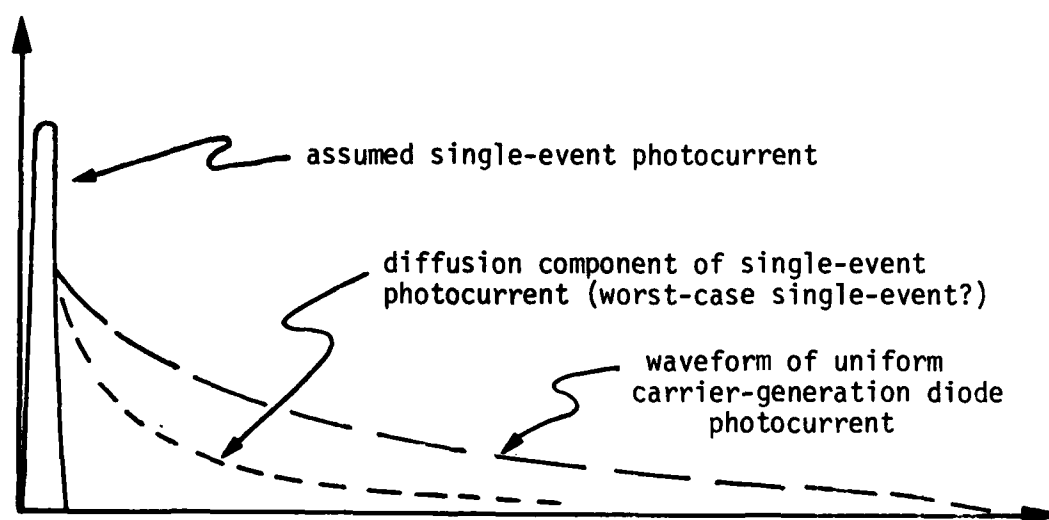waveform of uniform
carrier-generation diode
photocurrent

Figure 2.   Possible photocurrent waveforms.

The purpose of this analysis is to estimate the extent of the lateral carrier diffusion with the use of a simple two-dimensional model of carrier flow and collection.

A two-dimensional, cylindrically-symmetric bulk semiconductor region is shown in Figure 3. For this analysis we will approximate carrier densities by their average value over finite volumes. If a large number of small volumes were assumed this would simply be a finite-difference representation of the continuous equations of carrier distribution and flow. In this case, however, we know that the carrier distribution will vary strongly with distance near the junction and ionization track and more slowly with distance far into undisturbed bulk semiconductor. We therefore can select smaller volumes near the junction and ionization track and increase the volumes as we move out. In this way we can maintain reasonable accuracy in the analysis with a much simpler model.

For the region to be analyzed, as shown in Figure 3, we will assume that the reverse-biased p-n junction in in the x-r plane at $x = 0$ and the particle ionization track is down the center at $r = 0$.

The critical first-order semiconductor equations to be differenced are those relating minority carrier density, generation, recombination and diffusion in two dimensions. Assuming uniformly doped n-type material for the lumped volume at $x = i$ and $r = j$ we have,

$$i_{recomb._{i,j}} = qV_{i,j} (p_{i,j} - p_n)/\tau_p \tag{1}$$

for the carrier recombination where $V_{i,j}$ is the lumped element volume, $p_{i,j}$ is the average minority carrier density, $p_n$ is the thermal equilibrium minority carrier density, $\tau_p$ is the minority carrier lifetime. If we assume that the particle-induced carrier density is large compared to the thermal equilibrium value,
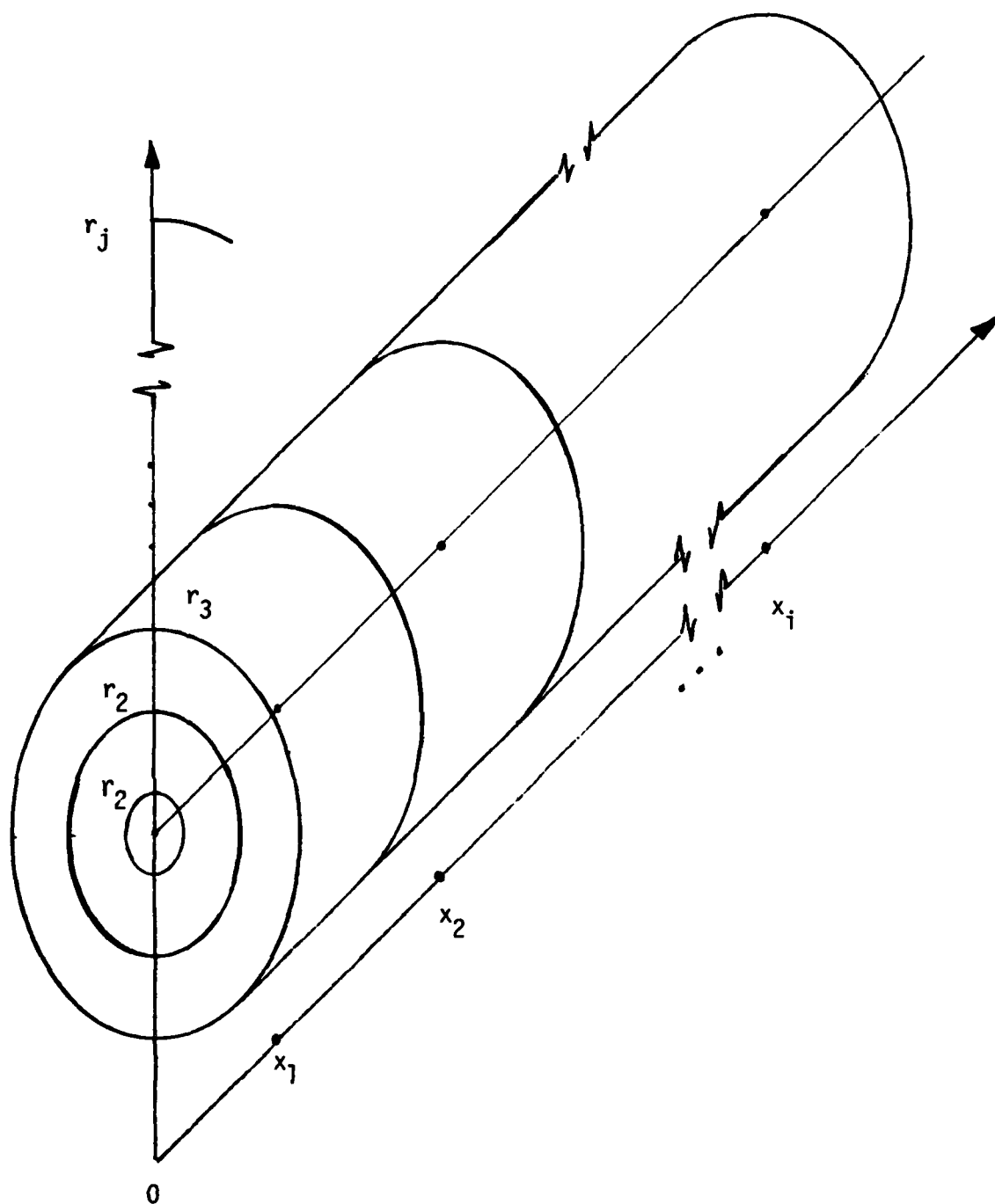
44

Figure 3. Two-dimensional cylindrically symmetrical bulk
semiconductor.

$$i_{recomb_{i,j}} \simeq (\frac{q\ V_{ij}}{\tau_p})\ p_{i,j} \tag{2}$$

Carrier generation in the lumped volume can be expessed as,

$$i_{gen_{i,j}} = (q\ V_{i,j})\ g_0(t) \tag{3}$$

where $g_0(t)$ is the induced time-dependent carrier generation rate. In this analysis, this term will be included only in the lumped elements along the x-axis.

Increase and decrease in carrier density in the lumped element can be represented by a carrier storage term as,

$$i_{storage_{i,j}} = (q\ V_{i,j})(dp_{i,j}/dt) \tag{4}$$

Carrier diffusion may be either axial or radial. For this term the current flow is determined by the difference in average value of carrier density in contiguous elements and the spacing between the central points of the elements. Axial diffusion current is then approximately:

$$i_{diffusion_{i,i+j,\ j}} = (\frac{qA_x D_p}{\Delta x_{i,i+1}})(P_{i,j} - p_{i+1,j}) \tag{5}$$

between the ith and (i+1)th elements where $A_x$ is the area of the axial interface and $D_p$ is the minority carrier diffusion constant. Similarly, for the radial current,

$$i_{diffusion_{i;j,j+1}} = (\frac{q\ A_r D_p}{\Delta r_{j,j+1}})\ (p_{i,j} - p_{i,j+1}) \tag{6}$$

46

Finally, the boundary condition between carrier density and junction voltage is established at the junction by

$$p_{x=0;r} = p_n[\exp\left(\frac{qV}{kT}\right) - 1]$$  (7)

where V is the applied junction voltage and the boundary condition is considered uniform across the junction plane.

Reviewing Equation 1-6 each involves constants of the bulk semiconductor, area, and lumped geometry multiplied by terms of the minority carrier density. Linvill defined these collective constants be terms and symbols (Ref. 4). Thus a lumped model network could be defined in terms of carrier density, current and voltage as shown in Figure 4 for a one-dimensional model. In general, the lumped-model can be used to represent carrier flow by drift as well as diffusion.

The lumped model network generally has fewer nodes than a finite-difference model but often still has too many for convenient closed form solution. A wide variety of circuit analysis computer programs is available for the analysis of linear and non-linear networks. Unfortunately, the electrical circuit network codes deal only in terms of current and voltage while the general lumped model network must involve current, voltage and carrier density [NET-2 has a provision of direct analysis of a limited set of lumped model networks but this provision is not widely used or easily available] (Ref. 5).

For this analysis, the difficulty can be resolved because we will assume that the junction is always reverse biased. The excess minority carrier density is then fixed at zero at the junction and the actual junction voltage is not a necessary parameter for the analysis. Now the only parameters of the lumped model analysis are minority carrier density and current. An electrical network can now be defined by considering the minority
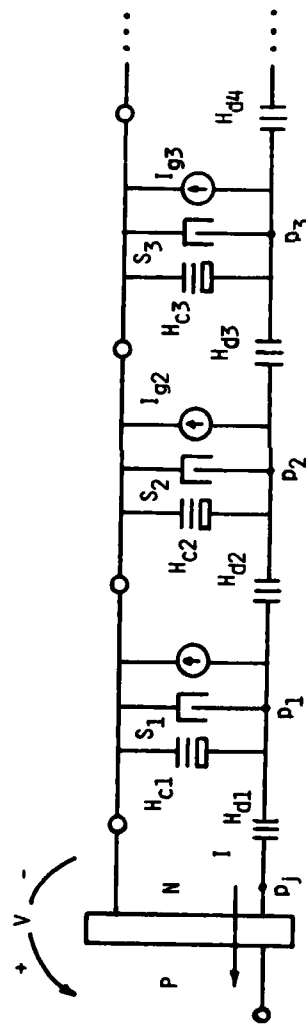
$$p_j = p_n \left[ \exp\left(\frac{qV}{kT}\right) - 1 \right]$$

$$H_{ci} = qV_i/\tau_p$$

$$H_{di} = qAD_p/W$$

$$S_i = qV_i$$

$$I_{gi} = qV_i g_0 \dot{\gamma}$$

Figure 4. One-dimensional lumped model.

carrier density as a "voltage". The junction photocurrent will be the calculated current that flows through a short-circuit at the junction. An electrically equivalent network for a two-dimensional model is shown in Figure 5.

The lumped model of Figure 5 approximates the bulk semiconductor volume by five regions along the x-axis and five radial volumes. The geometry was scaled in units of the minority carrier diffusion length $L_p$. The points of average carrier density for the axial and radial dimensions were selected as shown in Table I. As discussed previously the points are spaced

**Table I. Coordinates for Average Values of Carrier Density.**

$$x_1 = 0.1 \, L_p \qquad r_1 = 0.1 \, L_p$$

$$x_2 = 0.2 \, L_p \qquad r_2 = 0.2 \, L_p$$

$$x_3 = 0.3 \, L_p \qquad r_3 = 0.3 \, L_p$$

$$x_4 = 0.5 \, L_p \qquad r_4 = 0.5 \, L_p$$

$$x_5 = 0.8 \, L_p \qquad r_5 = 0.8 \, L_p$$

closer near the junction and center axis to preserve accuracy with a relatively small number of lumped regions (Ref. 6). The volumes associated with each lumped region are presented in Table II. In each as we have,

$$V_{x,r} = \pi \, (x_{i+1} - x_i)(r_{j+1}^2 - r_j^2) \tag{7}$$

In terms of the circuit network the value of the carrier recombination "conductances" is
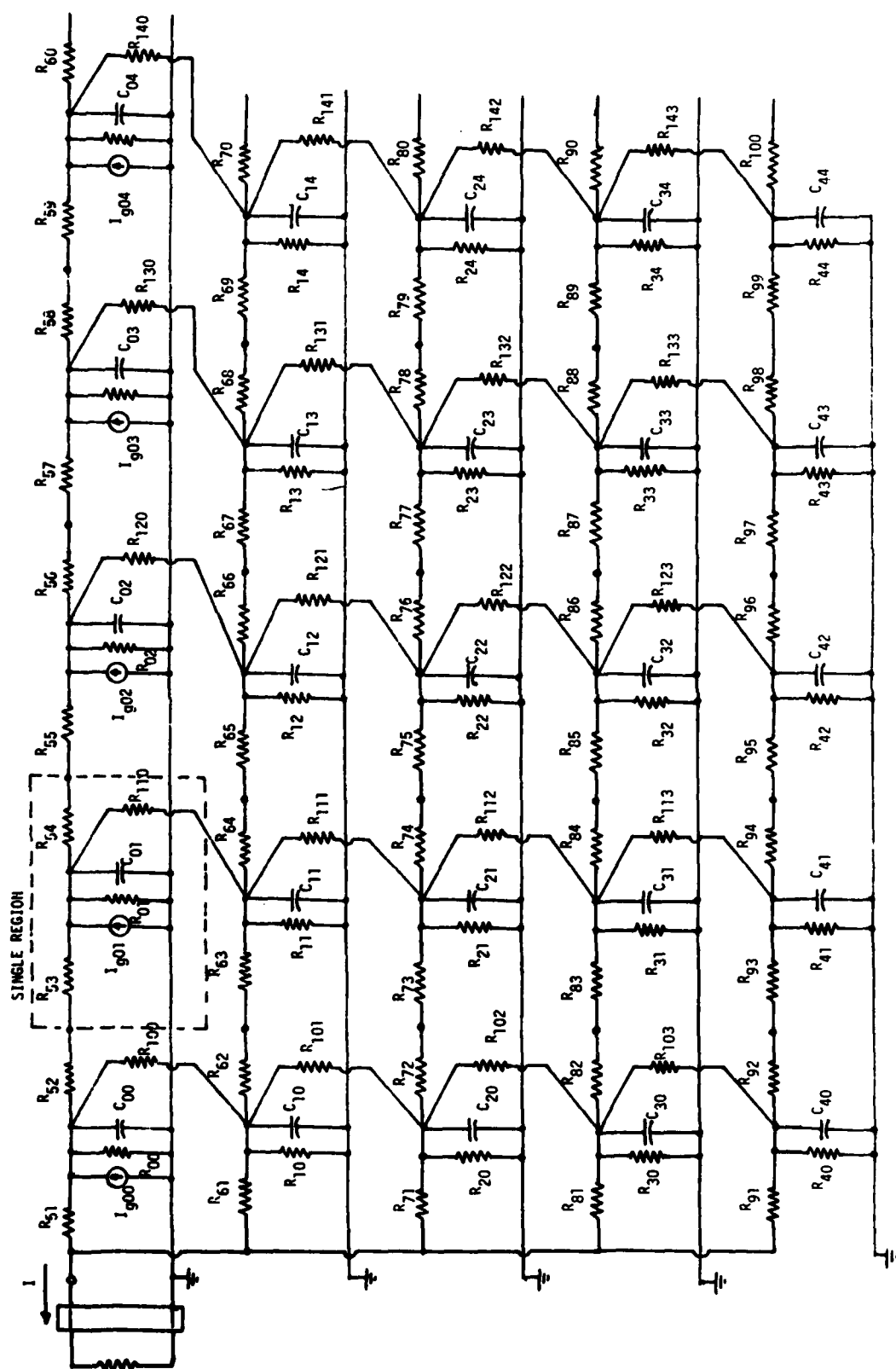
$$G_{x,r} = q \, V_{x,r}/\tau_p \text{ mhos.}$$

Figure 5. Two dimensional equivalent lumped model.

### Table II. Lumped Model Volumes in Units of $\pi L^3$

| r | 0 | 1 | 2 | 3 | 4 |
|---|---|---|---|---|---|
| x | 0.001 | 0.003 | 0.005 | 0.016 | 0.039 |
| 1 | 0.001 | 0.003 | 0.005 | 0.016 | 0.039 |
| 2 | 0.001 | 0.003 | 0.005 | 0.016 | 0.039 |
| 3 | 0.002 | 0.006 | 0.01 | 0.032 | 0.078 |
| 4 | 0.003 | 0.009 | 0.015 | 0.048 | 0.117 |

The value of the equivalent network capacitance is,

$$C_{x,r} = q \, V_{x,r} \text{ farads}$$

The values of the "conductances" representing conduction between elements are presented in Table III in terms of the element numbers as shown in Figure 5.

For the circuit response calculation the linear series conductances can be combined to reduce the number of elements. The equivalent circuit used is shown in Figure 6 with the parameter values used listed in Table IV.

Two calculations were made with the use of this model to get some insight into the contribution of two-dimensional carrier flow: one case was with the full network and the other was a one-dimensional network with the lateral diffusion conductances were removed. In both cases the carrier generation terms were assumed to be a 11 ns pulse. This, of course, is too long to be a realistic single particle ionization but the relative one- and two-dimensional effects should still be illustrated.

The calculated transient junction current is shown in Figure 7 for the one- and two-dimensional cases. It is seen that the variation between the two is small ($\approx$10%) and the one-dimensional approximation used in many analyses seems reasonable.

### Table III. Lumped Model Conductances in Units of $q_\pi L$ (mhos).

| | | | | |
|---|---|---|---|---|
| $G_{51} = 0.2$ | $G_{61} = 0.6$ | $G_{71} = 1.0$ | $G_{81} = 3.2$ | $G_{91} = 7.8$ |
| $G_{52} = 0.2$ | $G_{62} = 0.6$ | $G_{72} = 1.0$ | $G_{82} = 3.2$ | $G_{92} = 7.8$ |
| $G_{53} = 0.0667$ | $G_{63} = 0.2$ | $G_{73} = 0.33$ | $G_{83} = 1.067$ | $G_{93} = 2.6$ |
| $G_{54} = 0.0667$ | $G_{64} = 0.2$ | $G_{74} = 0.33$ | $G_{84} = 1.067$ | $G_{94} = 2.6$ |
| $G_{55} = 0.04$ | $G_{65} = 0.12$ | $G_{75} = 0.20$ | $G_{85} = 0.64$ | $G_{95} = 1.56$ |
| $G_{56} = 0.04$ | $G_{66} = 0.12$ | $G_{76} = 0.20$ | $G_{86} = 0.64$ | $G_{96} = 1.56$ |
| $G_{57} = 0.025$ | $G_{67} = 0.075$ | $G_{77} = 0.125$ | $G_{87} = 0.40$ | $G_{97} = 0.975$ |
| $G_{58} = 0.025$ | $G_{68} = 0.075$ | $G_{78} = 0.125$ | $G_{88} = 0.40$ | $G_{98} = 0.975$ |
| $G_{59} = 0.0154$ | $G_{69} = 0.046$ | $G_{79} = 0.077$ | $G_{89} = 0.246$ | $G_{99} = 0.6$ |
| $G_{60} = 0.0154$ | $G_{70} = 0.046$ | $G_{80} = 0.077$ | $G_{90} = 0.246$ | $G_{100} = 0.6$ |

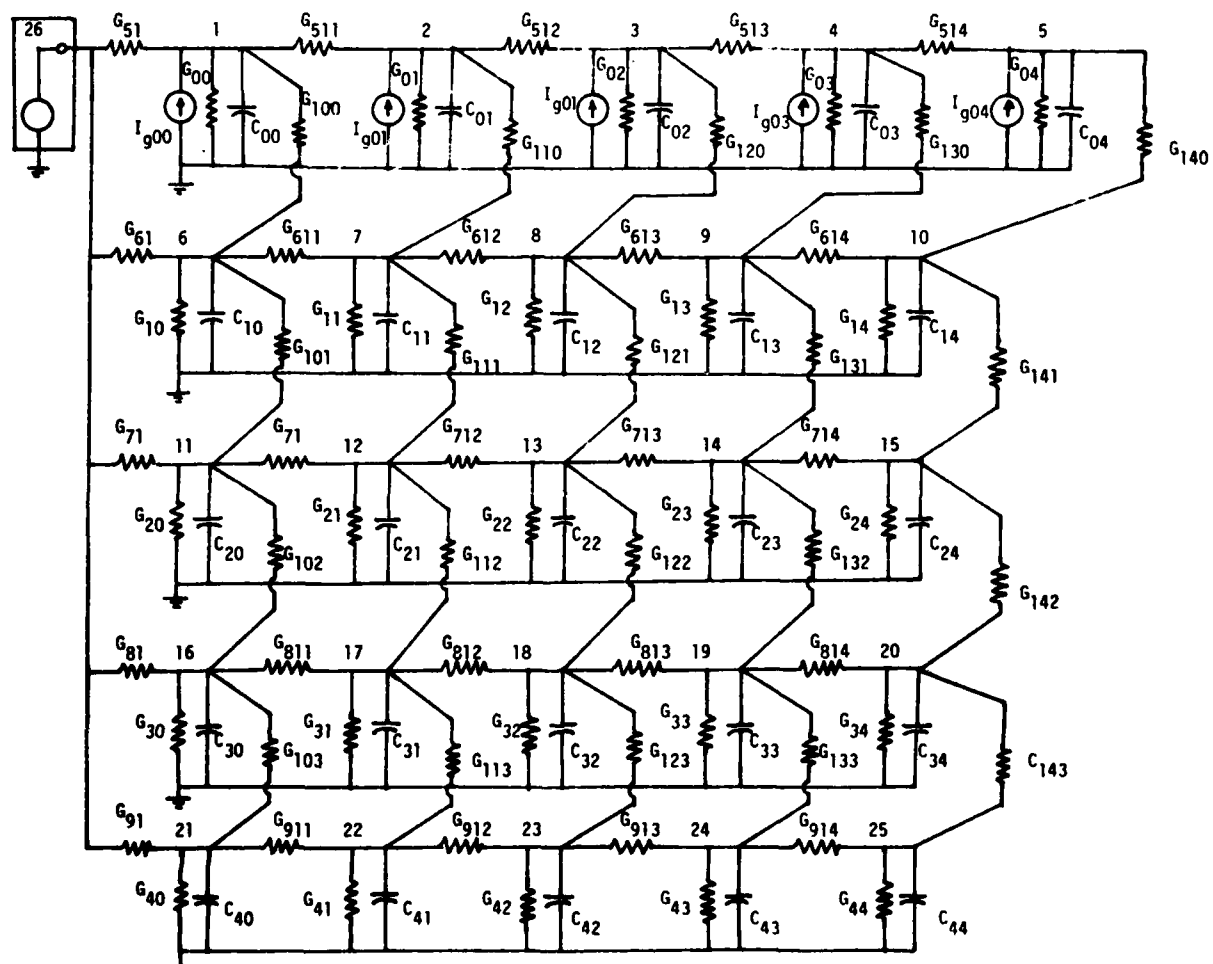| | | | |
|---|---|---|---|
| $G_{110} = 0.2$ | $G_{101} = 0.4$ | $G_{102} = 0.4$ | $G_{103} = 0.4$ |
| $G_{120} = 0.2$ | $G_{111} = 0.4$ | $G_{112} = 0.4$ | $G_{113} = 0.4$ |
| $G_{130} = 0.4$ | $G_{121} = 0.4$ | $G_{122} = 0.4$ | $G_{123} = 0.4$ |
| $G_{140} = 0.6$ | $G_{131} = 0.8$ | $G_{132} = 0.8$ | $G_{133} = 0.8$ |
| | $G_{141} = 1.2$ | $G_{142} = 1.2$ | $G_{143} = 1.2$ |

Figure 6. Single-event 2-D photoresponse model.

## Table IV. Circuit Description Single Event 2-d Photoresponse.

$G_{51} = 0.04$ mhos

$G_{511} = 0.01$ mhos

$G_{512} = 0.005$ mhos

$G_{513} = 0.0031$ mhos

$G_{514} = 0.002$ mhos


$G_{100} = 0.04$ mhos

$G_{110} = 0.04$ mhos

$G_{120} = 0.04$ mhos

$G_{130} = 0.08$ mhos

$G_{140} = 0.12$ mhos


$G_{61} = 0.12$ mhos

$G_{611} = 0.03$ mhos

$G_{612} = 0.015$ mhos

$G_{613} = 0.0092$ mhos

$G_{614} = 0.0058$ mhos


$G_{101} = 0.08$ mhos

$G_{111} = 0.08$ mhos

$G_{121} = 0.08$ mhos

$G_{131} = 0.16$ mhos

$G_{141} = 0.24$ mhos


$G_{/1} = 0.2$ mhos

$G_{/11} = 0.05$ mhos

$G_{/12} = 0.025$ mhos

$G_{/13} = 0.0154$ mhos


$C_{00} = 2.0 \times 10^{-10}$ F $= C_{01} = C_{02}$

$I_{00} = 1 \times 10^{-3}$ A $\cdot f(t) = I_{01} = I_{02}$

$G_{00} = 0.0002$ mhos $= G_{01} = G_{02}$

$C_{03} = 4 \times 10^{-10}$ F

$I_{03} = 2 \times 10^{-3}$ A $\cdot f(t)$

$G_{03} = 0.0004$ mhos

$C_{04} = 6.0 \times 10^{-10}$ F

$I_{04} = 3 \times 10^{-3}$ A $\cdot f(t)$

$G_{04} = 0.0006$ mhos


$C_{10} = 6 \times 10^{-10}$ F $= C_{11} = C_{12}$

$G_{10} = 0.0006$ mhos $= G_{11} = G_{12}$

$C_{13} = 1.2 \times 10^{9}$ F

$G_{13} = 0.0012$ mhos

$C_{14} = 1.8 \times 10^{-9}$ F

$G_{14} = 0.0018$ mhos


$C_{20} = 1 \times 10^{-9}$ F $= C_{21} = C_{22}$

$G_{20} = 0.001$ mhos $= G_{21} = G_{22}$

$C_{23} = 2 \times 10^{-9}$ F

$G_{23} = 0.002$ mhos

$C_{24} = 3 \times 10^{-9}$ F

$G_{24} = 0.003$ mhos

## Table IV. Continued.

$G_{81} = 0.64$ mhos

$G_{811} = 0.16$ mhos

$G_{812} = 0.08$ mhos

$G_{813} = 0.049$ mhos

$G_{814} = 0.03$ mhos

$C_{30} = 3.2 \times 10^{-9}$ F $= C_{31} = C_{32}$

$G_{30} = 0.0032$ mhos $= G_{31} = G_{32}$

$C_{33} = 6.4 \times 10^{-9}$ F

$G_{33} = 0.0064$ mhos

$C_{34} = 9.6 \times 10^{-9}$ F

$G_{34} = 0.0096$ mhos


$G_{102} = 0.08$ mhos

$G_{112} = 0.08$ mhos

$G_{122} = 0.08$ mhos

$G_{132} = 0.16$ mhos

$G_{142} = 0.24$ mhos

$C_{40} = 7.8 \times 10^{-9}$ F $= C_{41} = C_{42}$

$G_{40} = 0.078$ mhos $= G_{41} = G_{42}$

$C_{43} = 1.56 \times 10^{-8}$ F

$G_{43} = 0.0156$ mhos

$C_{44} = 2.34 \times 10^{-8}$ F


$G_{91} = 1.56$ mhos

$G_{911} = 0.39$ mhos

$G_{912} = 0.195$ mhos

$G_{913} = 0.12$ mhos

$G_{914} = 0.074$ mhos

$G_{103} = 0.08$ mhos

$G_{113} = 0.08$ mhos

$G_{123} = 0.08$ mhos
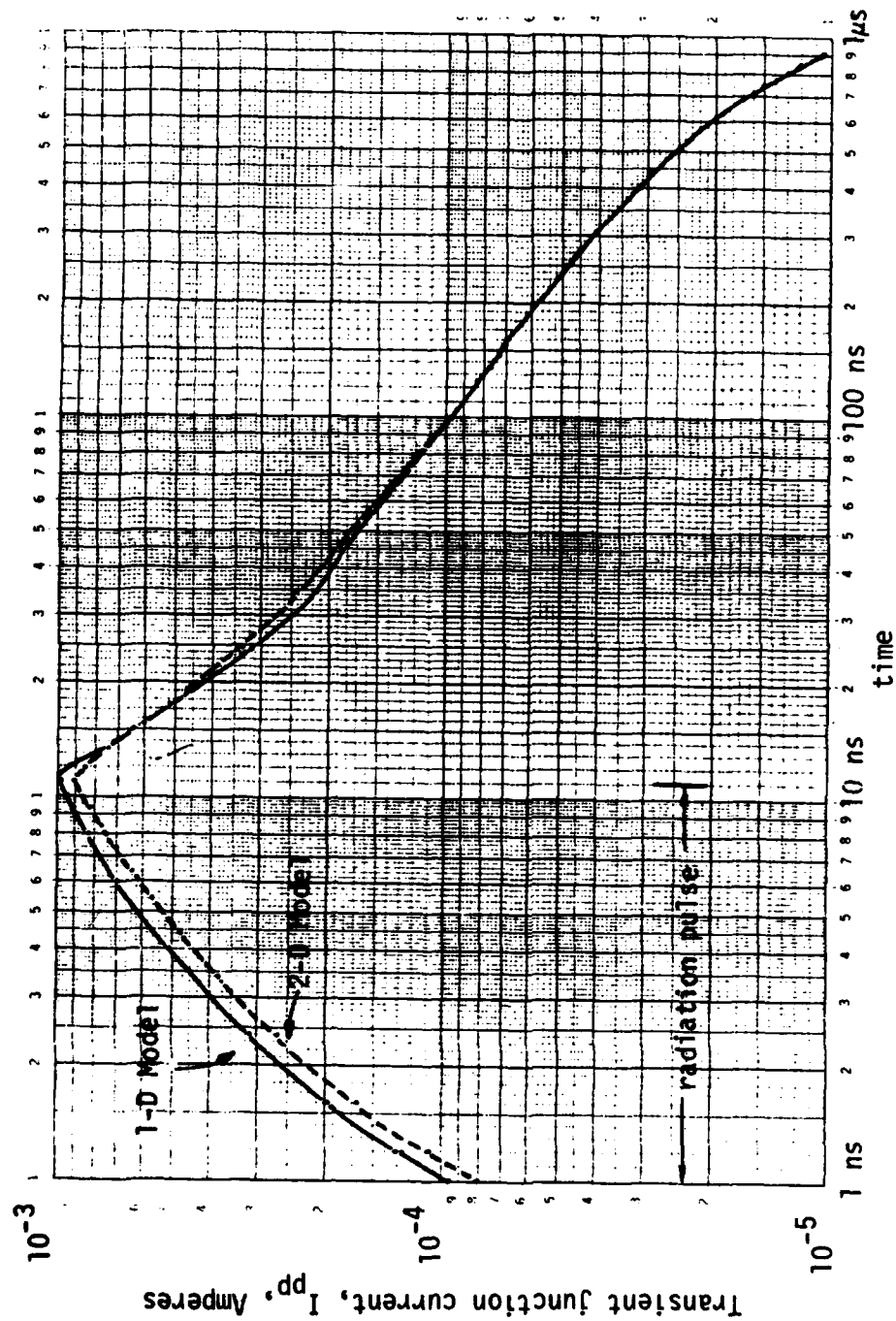
$G_{133} = 0.16$ mhos

$G_{143} = 0.24$ mhos

Figure 7.  Calculated transient junction current for 2-D and 1-D model.

# REFERENCES

1. C. Hu, "Alpha-Particle-Induced Field and Enhanced Collection of Carriers," IEEE Electron Device Letters, vol. EDL-3, no. 2, pp. 31-34; February 1982.

2. C. Hu, "Drift Collection of Alpha-Generated Carriers and Design Implications," ISSCC Digest of Papers, pp. 18-19, February 1982.

3. G.A. Sai-Halsz, "Alpha-Particle-Induced Soft Error Modeling," ibid, pp. 20-22.

4. J.G. Linvill and J.F. Gibbons, Transistors and Active Circuits, McGraw-Hill, 1961.

5. J.P. Raymond and M.G. Krebs, "Lumped Model Analysis of Semiconductor Devices Using the NET-2 Circuit/System Analysis Program," IEEE Trans. on Nuc. Sci., NS-19, no. 6, pp. 103-107; December 1972.

6. J.P. Raymond and J. Willis, "Lumped Models of Transistors and Diodes," IEEE Trans. on Nuc. Sci., NS-12, pp. 55-68, October, 1965.

# DISTRIBUTION LIST

DEPARTMENT OF DEFENSE

Assistant to the Secretary of Defense
Atomic Energy
    ATTN: Executive Assistant

Defense Intelligence Agency
    ATTN: DT-1C
    ATTN: DB-4N
    ATTN: DB-4C, E. O'Farrell

Defense Nuclear Agency
    ATTN: STSP
2 cy ATTN: SPSS
4 cy ATTN: TITL

Defense Technical Information Center
12 cy ATTN: DD

Field Command
Defense Nuclear Agency
    ATTN: FCTT, G. Ganong
    ATTN: FCTK
    ATTN: FCTXE
    ATTN: FCTT, W. Summa
    ATTN: FCPR

Field Command
DNA Det 1
Lawrence Livermore Lab
    ATTN: FC-1

Interservice Nuclear Weapons School
    ATTN: TTV

Joint Strat Tgt Planning Staff
    ATTN: NRI-STINFO, Library
    ATTN: JLA, Threat Applications Div

Under Secretary of Defense for Rsch & Engrg
    ATTN: Strategic & Space Sys (OS)
    ATTN: Strat & Thtr Nuc Forces, B. Stephan

DEPARTMENT OF THE ARMY

Chief of Engineers
Department of the Army
    ATTN: DAEN-RDL
    ATTN: DAEN-MPE-T

Harry Diamond Laboratories
Department of the Army
    ATTN: 00100 Commander/Tech Dir/Div Dir
    ATTN: DELHD-NW-P

U.S. Army Ballistic Research Labs
    ATTN: DRDAR-BLT, W. Taylor
    ATTN: DRDAR-BLT, J. Keefer
    ATTN: DRDAR-TSB-S

U.S. Army Concepts Analysis Agency
    ATTN: CSSA-ADL

U.S. Army Engineer Center & Ft Belvoir
    ATTN: DT-LRC

DEPARTMENT OF THE ARMY (Continued)

U.S. Army Engineer Div, Huntsville
    ATTN: HNDED-SR

U.S. Army Engineer Div, Ohio River
    ATTN: ORDAS-L

U.S. Army Engr Waterways Exper Station
    ATTN: WESSE
    ATTN: WESSD, J. Jackson
    ATTN: J. Strange
    ATTN: Library
    ATTN: WESSA, W. Flathau

U.S. Army Material & Mechanics Rsch Ctr
    ATTN: Technical Library

U.S. Army Materiel Dev & Readiness Cmd
    ATTN: DRXAM-TL

U.S. Army Missile Command
    ATTN: Doc Sec

U.S. Army Nuclear & Chemical Agency
    ATTN: Library

DEPARTMENT OF THE NAVY

Naval Research Laboratory
    ATTN: Code 2627

Naval Sea Systems Command
    ATTN: SEA-09G53, Library

Naval Surface Weapons Center
    ATTN: Code F31

Naval Surface Weapons Center
    ATTN: Tech Library & Info Svcs Br

Naval War College
    ATTN: Code E-11

Naval Weapons Evaluation Facility
    ATTN: Code 10

Office of Naval Research
    ATTN: Code 474, N. Perrone

Office of the Dep Chief of Naval Ops
    ATTN: NOP 981
    ATTN: OP 03EG

Strategic Systems Project Office
Department of the Navy
    ATTN: NSP-43

David Taylor Naval Ship R&D Ctr
    ATTN: Code L42-3 Library

Naval Electronic Systems Command
    ATTN: PME 117-21

Naval Facilities Engineering Command
    ATTN: Code 04B

DEPARTMENT OF THE NAVY (Continued)

Naval Material Command
    ATTN: MAT 08T-22

Naval Postgraduate School
    ATTN: Code 1424, Library

DEPARTMENT OF THE AIR FORCE

Air Force
    ATTN: INT

Air Force Institute of Technology
    ATTN: Library

Air Force Systems Command
    ATTN: DLW

Air force Weapons Lab
    ATTN: NTES-R
    ATTN: NTE
    ATTN: SUL

Air University Library
    ATTN: AUL-LSE

Ballistic Missile Office
    ATTN: ENSN, M. Furbee

Deputy Chief of Staff
Research, Development, & Acq
    ATTN: AFRDQI

Deputy Chief of Staff, Logistics & Engrg
    ATTN: LEEE

Foreign Technology Division
    ATTN: NIIS Library

Rome Air Development Center
    ATTN: TSLD

Strategic Air Command
    ATTN: NRI-STINFO Library

DEPARTMENT OF ENERGY

Department of Energy
    ATTN: CTID

Department of Energy
    ATTN: Doc Con for Tech Library

OTHER GOVERNMENT AGENCIES

Central Intelligence Agency
    ATTN: OSWR/NED

Department of Interior
Bureau of Mines
    ATTN: Tech Lib

Department of the Interior
US Geological Survey
    ATTN: D. Roddy

NATO

NATO School, SHAPE
    ATTN: US Documents Officer

DEPARTMENT OF ENERGY CONTRACTORS

University of Calfornia
Lawrence Livermore National Lab
    ATTN: Tech Info Dept Library
    ATTN: L-10, H. Kruger
    ATTN: W. Crowley
    ATTN: D. Burton

Los Alamos National Lab
    ATTN: MS420, N. Hoffman
    ATTN: Reports Library
    ATTN: B. Killian
    ATTN: MS530, G. Spillman

Oakridge National Lab
    ATTN: Civil Def Res Proj
    ATTN: Central Rsch Library

Sandia National Lab
    ATTN: L. Vortman
    ATTN: Org 7112, A. Chabai
    ATTN: Tech Lib 3141

Sandia National Labs, Livermore
    ATTN: Library & Security Classification Div

DEPARTMENT OF DEFENSE CONTRACTORS

Aerospace Corp
    ATTN: Tech Info Services

Agbabian Associates
    ATTN: M. Agbabian

Applied Research Associates, Inc
    ATTN: N. Higgins
    ATTN: J. Bratton

Applied Research Associates, Inc
    ATTN: S. Blouin

Applied Research Associates, Inc
    ATTN: D. Piepenburg

Applied Research Associates, Inc
    ATTN: B. Frank

Applied Theory, Inc
    ATTN: J. Trulio

AVCO Systems Division
    ATTN: Library A 830

BDM Corp
    ATTN: T. Neighbors
    ATTN: Corporate Library

BDM Corp
    ATTN: F. Leech
4 cy ATTN: L. Walker
4 cy ATTN: E. Bultman

Boeing Aerospace Co
    ATTN: MS/42-37, R. Schmidt

Boeing Co
    ATTN: Aerospace Library

California Institute of Technology
    ATTN: T. Ahrens

DEPARTMENT OF DEFENSE CONTRACTORS (Continued)

California Research & Tech, Inc
    ATTN: S. Schuster
    ATTN: Library
    ATTN: K. Kreyenhagen

California Research & Tech, Inc
    ATTN: D. Orphal

Calspan Corp
    ATTN: Library

University of Denver
    ATTN: Sec Officer for J. Wisotski

EG&G Wash Analytical Svcs Ctr, Inc
    ATTN: Library

Electro-Mech Systems , Inc
    ATTN: R. Shunk

Energy Systems, Inc
    ATTN: W. Ogle

Gard, Inc
    ATTN: G. Neidhardt

Horizons Tech, Inc
    ATTN: R. Kruger

IIT Research Institute
    ATTN: Doc Library

Institute for Defense Analyses
    ATTN: Classified Library

Kaman AviDyne
    ATTN: Library

Kaman Sciences Corp
    ATTN: Library

Kaman Tempo
    ATTN: DASIAC

Lockheed Missiles & Space Co, Inc
    ATTN: T. Geers
    ATTN: Tech Info Center

Lockheed Missiles & Space Co, Inc
    ATTN: TIC-Library

McDonnell Douglas Corp
    ATTN: R. Halprin

Mission Research Corp
4 cy ATTN: R. Pease
4 cy ATTN: J. Raymond

Mission Research Corp
5 cy ATTN: Doc Con

Merritt Cases, Inc
    ATTN: Library
    ATTN: J. Merritt

University of New Mexico
    ATTN: N. Baum

Pacifica Technology
    ATTN: Tech Library

Pacific-Sierra Research Corp
    ATTN: L. Schlessinger
    ATTN: H. Brode, Chairman SAGE

Patel Enterprises, Inc
    ATTN: M. Patel

Physics International Co
    ATTN: L. Behrmann
    ATTN: E. Moore
    ATTN: F. Sauer
    ATTN: Technical Library
    ATTN: J. Thomsen

R&D Associates
    ATTN: W. Wright
    ATTN: R. Port
    ATTN: J. Lewis
    ATTN: Tech Info Center
    ATTN: J. Carpenter

S-CUBED
    ATTN: K. Pyatt
    ATTN: R. Lafrenz
    ATTN: T. Riney
    ATTN: D. Grine
    ATTN: Library
    ATTN: T. Cherry

Science Applications, Inc
    ATTN: Tech Library
    ATTN: H. Wilson
    ATTN: M. McKay

Science Applications, Inc
    ATTN: D. Maxwell
    ATTN: D. Bernstein

Science Applications, Inc
    ATTN: W. Layson

Southwest Research Institute
    ATTN: A. Wenzel
    ATTN: W. Baker

SRI International
    ATTN: J. Colton
    ATTN: G. Abrahamson

Structural Mechanics Associates, Inc
    ATTN: R. Kennedy

Teledyne Brown Engineering
    ATTN: D. Ormond
    ATTN: F. Leopard
    ATTN: J. Ford

Terra Tek, Inc
    ATTN: Library
    ATTN: S. Green

Tetra Tech, Inc
    ATTN: L. Hwang

TRW Electronics & Defense Sector
    ATTN: Tech Info Center
    ATTN: D. Baer
    ATTN: R. Plebuch
2 cy ATTN: N. Lipner

DEPARTMENT OF DEFENSE CONTRACTORS (Continued)

TRW Electronics & Defense Sector
    ATTN:  P. Dai
    ATTN:  E. Wong

Universal Analytics, Inc
    ATTN:  E. Field

DEPARTMENT OF DEFENSE CONTRACTORS (Continued)

Weidlinger Assoc, Consulting Engrg
    ATTN:  J. Wright
    ATTN:  M. Baron

Weidlinger Associates
    ATTN:  J. Isenberg